Argonne NATIONAL LABORATORY

ANL-GenIV-103

Performance Improvement Options for the Supercritical Carbon Dioxide Brayton Cycle

Nuclear Engineering Division

About Argonne National Laboratory
Argonne is a U.S. Department of Energy laboratory managed by UChicago Argonne, LLC under contract DE-AC02-06CH11357. The Laboratory's main facility is outside Chicago, at 9700 South Cass Avenue, Argonne, Illinois 60439. For information about Argonne, see www.anl.gov.

Availability of This Report
This report is available, at no cost, at http://www.osti.gov/bridge. It is also available on paper to the U.S. Department of Energy and its contractors, for a processing fee, from:

U.S. Department of Energy
Office of Scientific and Technical Information
P.O. Box 62
Oak Ridge, TN 37831-0062
phone (865) 576-8401
fax (865) 576-5728
reports@adonis.osti.gov

ANL-GenIV-103

Performance Improvement Options for the Supercritical Carbon Dioxide Brayton Cycle

by
A. Moisseytsev and J.J. Sienicki
Nuclear Engineering Division, Argonne National Laboratory

June 6, 2007

Table of Contents

List of Figures

List of Tables

Abstract

The supercritical carbon dioxide (S-CO_2) Brayton cycle is under development at Argonne National Laboratory as an advanced power conversion technology for Sodium-Cooled Fast Reactors (SFRs) as well as other Generation IV advanced reactors as an alternative to the traditional Rankine steam cycle. For SFRs, the S-CO_2 Brayton cycle eliminates the need to consider sodium-water reactions in the licensing and safety evaluation, reduces the capital cost of the SFR plant, and increases the SFR plant efficiency. Even though the S-CO_2 cycle has been under development for some time and optimal sets of operating parameters have been determined, those earlier development and optimization studies have largely been directed at applications to other systems such as gas-cooled reactors which have higher operating temperatures than SFRs. In addition, little analysis has been carried out to investigate cycle configurations deviating from the selected "recompression" S-CO_2 cycle configuration.

In this work, several possible ways to improve S-CO_2 cycle performance for SFR applications have been identified and analyzed. One set of options incorporates optimization approaches investigated previously, such as variations in the maximum and minimum cycle pressure and minimum cycle temperature, as well as a tradeoff between the component sizes and the cycle performance. In addition, the present investigation also covers options which have received little or no attention in the previous studies. Specific options include a "multiple-recompression" cycle configuration, intercooling and reheating, as well as liquid-phase CO_2 compression (pumping) either by CO_2 condensation or by a direct transition from the supercritical to the liquid phase.

Some of the options considered did not improve the cycle efficiency as could be anticipated beforehand. Those options include: a double recompression cycle, intercooling between the compressor stages, and reheating between the turbine stages. Analyses carried out as part of the current investigation confirm the possibilities of improving the cycle efficiency that have been indentified in previous investigations. The options in this group include: increasing the heat exchanger and turbomachinery sizes, raising of the cycle high end pressure (although the improvement potential of this option is very limited), and optimization of the low end temperature and/or pressure to operate as close to the (pseudo) critical point as possible. Analyses carried out for the present investigation show that significant cycle performance improvement can sometimes be realized if the cycle operates below the critical temperature at its low end. Such operation, however, requires the availability of a heat sink with a temperature lower than 30 ^{o}C for which applicability of this configuration is dependent upon the climate conditions where the plant is constructed (i.e., potential performance improvements are site specific). Overall, it is shown that the S-CO_2 Brayton cycle efficiency can potentially be increased to 45 %, if a low temperature heat sink is available and incorporation of larger components (e.g.., heat exchangers or turbomachinery) having greater component efficiencies does not significantly increase the overall plant cost.

1. Introduction

Previous analyses of supercritical carbon dioxide (S-CO_2) Brayton cycle power converters [1-10] have shown that the cycle has many advantages compared to the traditional Rankine steam cycle. The advantages include higher cycle efficiency, smaller components (especially, turbomachinery), fewer components, and simpler cycle layout. In order to realize the benefits of greater cycle efficiency, the CO_2 temperature at the turbine inlet should be sufficiently high [6]. Figure 1 shows that the S-CO_2 cycle has efficiency benefits over a superheated steam cycle at turbine inlet temperatures above 450 ^oC and above a supercritical water cycle above 550 ^oC. However, the results in Figure 1 were among the first results obtained for the S-CO_2 cycle; several practical aspects such as pressure drops in pipes and turbomachinery exit losses were ignored in that early study. More recent analyses [8-10] have shown that the S-CO_2 efficiency curve should be slightly lower than that shown in Figure 1. As a result, the S-CO_2 cycle achieves an efficiency higher than that of the superheated steam cycle at temperatures above ~480 ^oC.

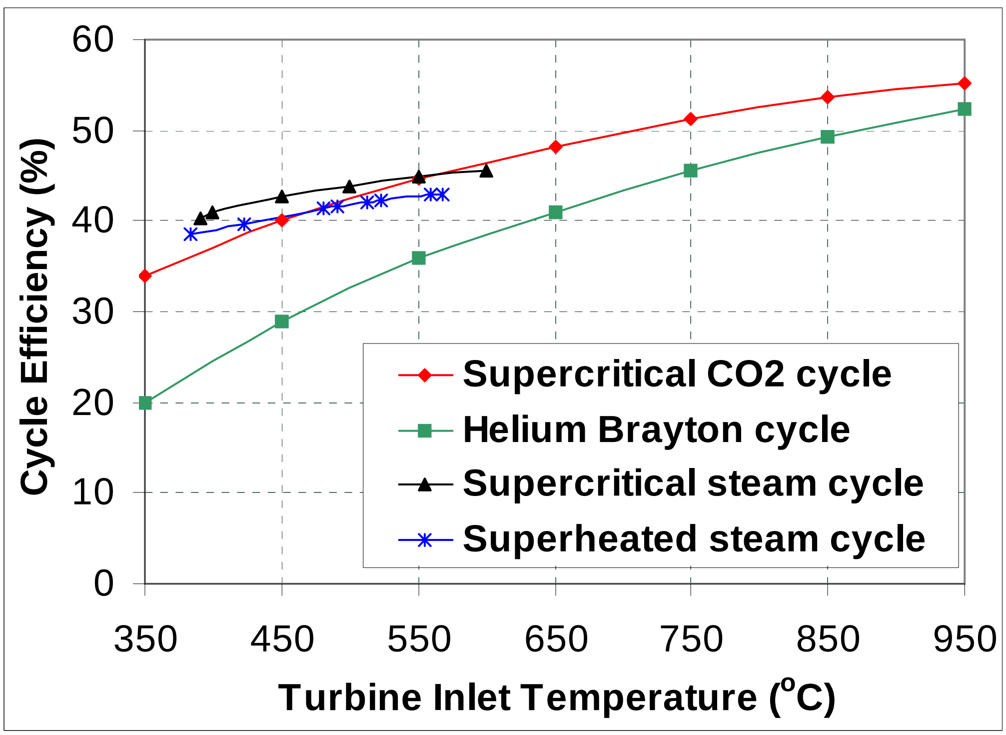

Figure 1. Cycle Efficiency Comparison of Advanced Power Cycles [6].

The recent focus of S-CO_2 cycle development under the Department of Energy Generation IV Nuclear Energy Systems Initiative has been the application of the cycle as a power converter for sodium-cooled fast reactors (SFRs). For a SFR, a typical core outlet temperature is about 500-550 ^oC. In addition, SFR's usually employ an intermediate sodium circuit with about 20-30 ^oC temperature drop from the primary to the intermediate loops. As a result, about 470 ^oC has been calculated for the S-CO_2

turbine inlet temperature when this cycle is coupled to a SFR [8,10]. According to Figure 1, the cycle efficiency benefits over the Rankine steam cycle are small, if even existent. Nonetheless, for these temperature limits, several other benefits of the cycle, such as lower capital cost, simpler cycle layout, and small turbomachinery still make the S-CO_2 cycle an attractive option as a power converter for a SFR. Most significantly, the S-CO_2 Brayton cycle eliminates the need to deal with sodium-water reactions in the licensing and safety evaluation. Indeed, the is the principal reason for considering the S-CO_2 Brayton cycle as an advanced power converter for SFRs.

The goal of the present study is to investigate potential tradeoffs between the cycle efficiency and other benefits of the S-CO_2 cycle. For example, it is realized that the majority of the plant capital cost comes from the reactor and intermediate loop systems. Therefore, it is worthwhile to investigate how much the S-CO_2 cycle efficiency for a SFR can be increased even if the cycle capital cost increases.

SFRs are usually designed for full load operation such that both reactor and power conversion system are usually highly optimized for operation at nominal power. In particular, the steam cycles for a SFR are usually very complex with several turbine stages and multiple steam extraction lines to achieve optimal performance at full power. If higher S-CO_2 cycle efficiency can be achieved even for a more complex cycle layout, the benefits for the whole plant might overcome the costs associated with the increase in complexity.

Several potential options to improve the S-CO_2 cycle efficiency have been identified as listed below. All these options explore to various extent the potential for improving the S-CO_2 cycle efficiency for a SFR versus increase in the cycle capital cost.

The options specifically considered in this work are:

- *Multiple recompression cycle*. The recompression cycle, which is now a reference S-CO_2 cycle, employs a splitting of the CO_2 flow to compensate for the variation in CO_2 properties with pressure. The recompression cycle shows the significant efficiency benefits over a simple cycle without flow splitting such that the question can be asked if multiple stages of recompression could be used to further enhance the cycle performance.

- *Optimization of the minimum cycle temperature and pressure*. The S-CO_2 cycle efficiency is very sensitive to the operating conditions at the bottom of the cycle. However, most previous analyses have been limited to supercritical conditions. In this report, other options are investigated such as a transition from supercritical conditions to subcritical conditions with a predominantly liquid phase either directly or though CO_2 condensation.

- *Intercooling cycles*. Intercooling between compressor stages is a common approach to increasing cycle efficiency for ideal gas Brayton cycles. Applicability of this approach to a S-CO_2 cycle needs to be determined.

- *Reheating cycle*. Similar to the intercooling between the compressor stages, reheating between turbine stages is a common approach for the Rankine cycle. An analysis is required to investigate the potential benefits for a S-CO_2 cycle.

- *Component size and optimization*. In previous analyses, the size of the components, such as heat exchanger volume and number of stages in turbomachinery, has been somewhat arbitrary selected mostly based on the trade-off between component cost and performance. It is realized, however, that there is a possibility of improving cycle performance provided by the specific features of the S-CO_2 cycle. For example, doubling the number of stages in the turbine to obtain an increase in cycle efficiency might still be cost effective if the cost of the small S-CO_2 turbine is sufficiently low.

The analysis of each of the above options is described in detail. The cycle improvement options are compared to a set of reference conditions for a SFR which are presented first in this document.

2. Reference Conditions

For the analyses presented in further sections, the S-CO_2 cycle conditions for the Advanced Burner Test Reactor (ABTR) have been selected [8]. The ABTR is designed for 250 MWt core power, which translates to about 100 MWe generator output. The sodium core inlet and outlet temperatures are 355 ^oC and 510 ^oC, respectively. There is a 22 ^oC temperature drop from the primary to the intermediate Na loop, so the intermediate sodium temperature at Na-to-CO_2 heat exchanger inlet is 488 ^oC. The S-CO_2 temperature at the turbine inlet is about 470 ^oC. The resulting cycle efficiency is 39 %. At the bottom of the cycle, the CO_2 is cooled such that when the flow accelerates at the compressor inlet nozzle, the static temperature and pressure are 31.25 ^oC and 7.40 MPa, which are very close to but still above the CO_2 critical point (30.98 ^oC and 7.373 MPa).

Table 1 shows the detailed design and nominal operating conditions for the S-CO_2 Brayton cycle components for the reference cycle. The cycle and each component optimization process are described in detail in Reference [8].

For this work, it is assumed that the conditions on sodium side (flow rate and temperatures) are fixed. Therefore, the S-CO_2 cycle itself is optimized be optimized for the fixed sodium side conditions. It is noted however that there remains an opportunity to improve both the cycle and entire plant performance by optimizing the sodium side conditions, as through variation of the intermediate sodium flow rate and the intermediate heat exchanger (IHX) inlet temperature. This additional joint optimization of both the power conversion cycle and the reactor heat transport system is beyond the scope of the current investigation.

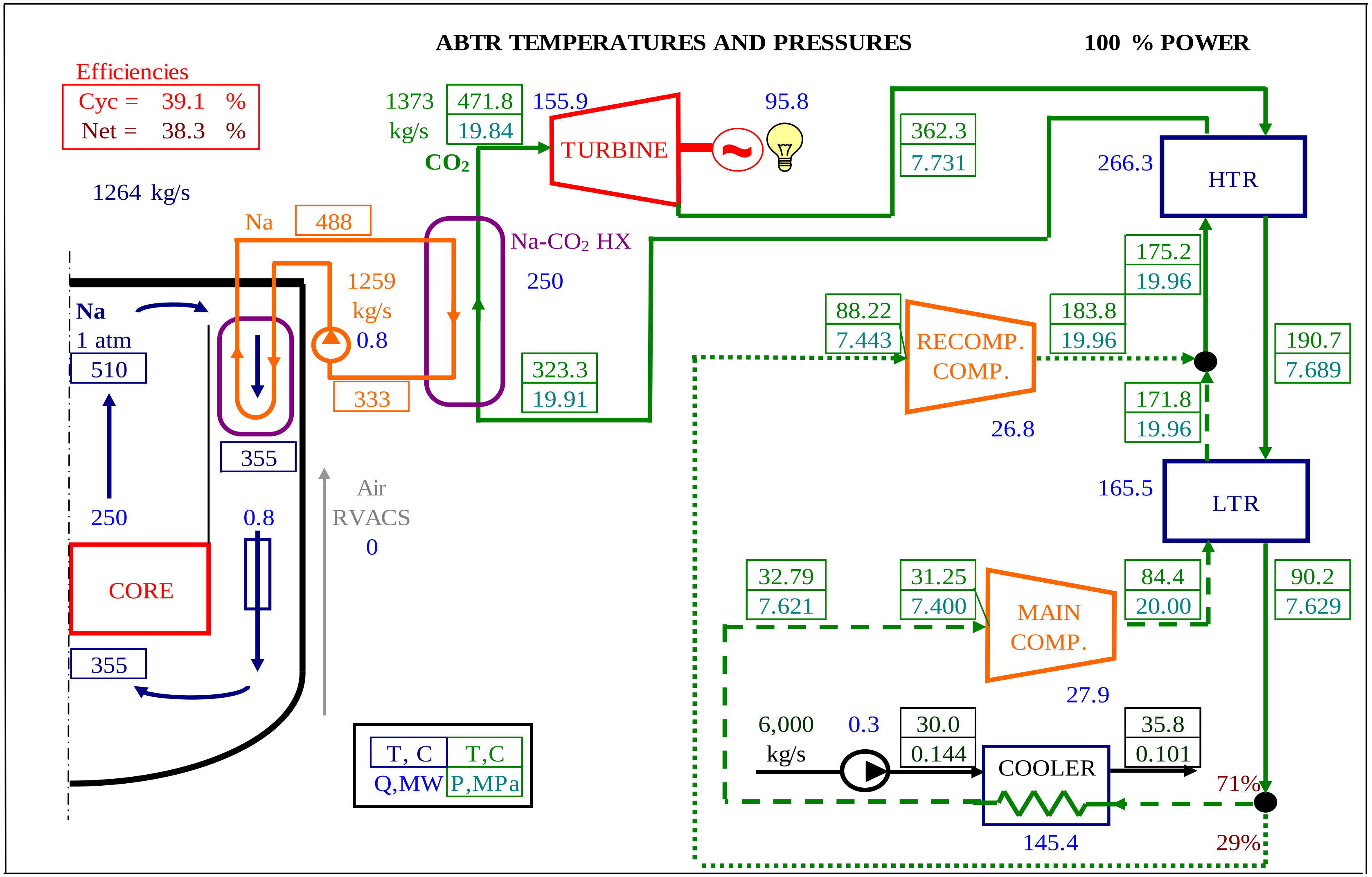

Figure 2. Reference S-CO_2 Brayton Cycle Conditions and Calculated Performance.

Table 1. Reference S-CO_2 Cycle Component Design and Nominal Operating Conditions

Division	Items	Spec. (SI)	Unit	Remarks
Na-CO2 Heat Exchanger	Type	PCHE		
	Quantity	64		All parameters below are per unit
	Heat transfer capacity	3.91	MWt	
	Heat transfer area	133.5	m2	
	Unit width	0.600	m	
	Unit height	0.600	m	
	Unit length	1.000	m	
	Heat transfer length	0.780	m	
	Plate material	SS316		
	Number of plates	141		Each side
	Number of Na channels	236		Per plate
	Na plate thickness	2.00	mm	
	Na channel diameter	2.0	mm	Semi-circular channel
	Na channel pitch	2.4	mm	
	Na channel length	0.780	m	Heat transfer region
	Na channel angle	0.0	deg	
	Number of CO2 channels	204		per plate
	CO2 plate thickness	2.00	mm	
	CO2 channel diameter	2.0	mm	Semi-circular channel
	CO2 channel pitch	2.4	mm	
	CO2 channel length	0.901	m	Heat transfer region
	CO2 channel angle	60.0	deg	
	Void fraction	30.9	%	From channels
	Sodium temperature inlet	488.0	C	
	Sodium temperature outlet	333.0	C	
	Sodium flow rate	19.7	kg/s	
	Pressure drop on Na side	2.5	kPa	
	Sodium inventory	34.9	kg	HT region only
	Sodium residence time	1.777	s	HT region only
	Sodium average speed	0.439	m/s	HT region only
	CO2 temperature inlet	323.4	C	
	CO2 temperature outlet	471.7	C	
	CO2 pressure inlet	19.907	MPa	
	CO2 pressure outlet	19.843	MPa	
	CO2 flow rate	21.5	kg/s	
	Effectiveness	94.2	%	
	Metal mass	1.854	tonnes	Dry
	Cost	111.3	K$	At $60/kg
	CO2 mass	6.5	kg	Operating conditions
High Temperature Recuperator	Type	PCHE		
	Quantity	64		All parameters below are per unit
	Heat transfer capacity	4.15	MWt	
	Heat transfer area	134.6	m2	
	Unit width	1.500	m	
	Unit height	0.600	m	
	Unit length	0.600	m	
	Heat transfer length	0.380	m	
	Channel diameter	1.5	mm	Semi-circular channel
	Channel pitch	2.3	mm	
	Plate thickness	2.0	mm	
	Plate material	SS316		
	Number of plates	141		Each side
	Hot side number of channels	564		Per plate
	Hot side channel length	0.439	m	Heat transfer region
	Hot side channel angle	60.0	deg	
	Cold side number of channels	461		Per plate
	Cold side channel length	0.537	m	Heat transfer region
	Cold side channel angle	90.0	deg	
	Void fraction	19.2	%	From channels
	Hot side temperature inlet	362.3	C	
	Hot side temperature outlet	191.1	C	
	Hot side pressure inlet	7.731	MPa	
	Hot side pressure outlet	7.690	MPa	

	Hot side flow rate	21.5	kg/s	
	Cold side temperature inlet	175.6	C	
	Cold side temperature outlet	323.4	C	
	Cold side pressure inlet	19.960	MPa	
	Cold side pressure outlet	19.907	MPa	
	Cold side flow rate	21.5	kg/s	
	Effectiveness	91.7	%	
	Metal mass	3.291	tonnes	Dry
	Cost	197.5	K$	At $60/kg
	CO2 mass	9.7	kg	Operating conditions
Low Temperature Recuperator	Type	PCHE		
	Quantity	128		All parameters below are per unit
	Heat transfer capacity	1.30	MWt	
	Heat transfer area	79.4	m2	
	Unit width	0.600	m	
	Unit height	0.600	m	
	Unit length	0.800	m	
	Heat transfer length	0.580	m	
	Channel diameter	1.5	mm	Semi-circular channel
	Channel pitch	2.3	mm	
	Plate thickness	2.0	mm	
	Plate material	SS316		
	Number of plates	141		Each side
	Hot side number of channels	218		Per plate
	Hot side channel length	0.670	m	Heat transfer region
	Hot side channel angle	60.0	deg	
	Cold side number of channels	178		Per plate
	Cold side channel length	0.820	m	Heat transfer region
	Cold side channel angle	90.0	deg	
	Void fraction	18.5	%	From channels
	Hot side temperature inlet	191.1	C	
	Hot side temperature outlet	90.3	C	
	Hot side pressure inlet	7.690	MPa	
	Hot side pressure outlet	7.629	MPa	
	Hot side flow rate	10.7	kg/s	
	Cold side temperature inlet	84.4	C	
	Cold side temperature outlet	172.2	C	
	Cold side pressure inlet	20.000	MPa	
	Cold side pressure outlet	19.960	MPa	
	Cold side flow rate	7.6	kg/s	
	Effectiveness	94.5	%	
	Metal mass	1.817	tonnes	Dry
	Cost	109.0	K$	At $60/kg
	CO2 mass	10.0	kg	Operating conditions
Cooler	Type	PCHE		
	Quantity	48		All parameters below are per unit
	Heat transfer capacity	3.03	MWt	
	Heat transfer area	199.2	m2	
	Unit width	1.500	m	
	Unit height	0.600	m	
	Unit length	0.593	m	
	Heat transfer length	0.373	m	
	Channel diameter	2.0	mm	Semi-circular channel
	Channel pitch	2.4	mm	
	Plate thickness	1.66	mm	
	Plate material	SS316		
	Number of plates	170		Each side
	CO2 side number of channels	432		Per plate
	CO2 side channel length	0.528	m	Heat transfer region
	CO2 side channel angle	90.0	deg	
	H2O side number of channels	529		Per plate
	H2O side channel length	0.431	m	Heat transfer region
	H2O side channel angle	90.0	deg	
	Void fraction	35.0	%	From channels
	CO2 temperature inlet	90.3	C	
	CO2 temperature outlet	32.79	C	
	CO2 pressure inlet	7.629	MPa	
	CO2 pressure outlet	7.621	MPa	
	CO2 flow rate	20.3	kg/s	

	Water temperature inlet	30.0	C	
	Water temperature outlet	35.8	C	
	Water pressure inlet	0.144	MPa	
	Water pressure outlet	0.101	MPa	
	Water flow rate	125.0	kg/s	
	Water pump power	0.286	MW	Total all units
	Effectiveness	95.4	%	
	Metal mass	2.729	tonnes	Dry
	Cost	163.7	K$	At $60/kg
	CO2 mass	16.2	kg	Operating conditions
Turbine	Type	Axial		
	Power	156.03	MW	
	Number of stages	6		
	Rotational speed	60.0	rev/s	
	Length (total)	2.66	m	Without casing
	Length (stages)	1.02	m	Without casing
	Length (diffuser)	1.64	m	
	Max diameter	0.87	m	Without casing
	Hub radius min	27.0	cm	
	Hub radius max	34.1	cm	
	Tip radius min	41.4	cm	
	Tip radius max	43.5	cm	
	Blade height min	7.3	cm	
	Blade height max	16.4	cm	
	Blade chord min	7.4	cm	
	Blade chord max	10.9	cm	
	Max Mach number	0.40		
	CO2 temperature inlet	471.7	C	
	CO2 temperature outlet	362.3	C	
	CO2 pressure inlet	19.84	MPa	
	CO2 pressure outlet	7.731	MPa	
	CO2 flow rate	1373.6	kg/s	
	Efficiency	93.4	%	Total-to-total
	CO2 mass	24.0	kg	Operating conditions
Compressor #1	Type	Centr.		
	Power	27.88	MW	
	Number of stages	1		
	Rotational speed	60.0	rev/s	
	Axial length	0.39	m	Without casing, estimated
	Max diameter	1.89	m	Without casing and volute
	Hub radius min	9.6	cm	
	Hub radius max	9.6	cm	
	Impeller radius min	57.0	cm	
	Impeller radius max	57.0	cm	
	Blade height min	1.5	cm	
	Blade height max	9.3	cm	
	Blade length min	23.1	cm	
	Blade length max	51.0	cm	
	Max Mach number	0.47		
	CO2 temperature inlet	32.79	C	
	CO2 temperature outlet	84.4	C	
	CO2 pressure inlet	7.621	MPa	
	CO2 pressure outlet	20.00	MPa	
	CO2 flow rate	975.3	kg/s	
	Efficiency	88.9	%	Total-to-static
	CO2 mass	59.3	kg	Operating conditions
Compressor #2	Type	Centr.		
	Power	26.92	MW	
	Number of stages	2		
	Rotational speed	60.0	rev/s	
	Axial length	0.48	m	Without casing, estimated
	Max diameter	2.04	m	Without casing and volute
	Hub radius min	20.3	cm	
	Hub radius max	21.0	cm	
	Impeller radius min	59.0	cm	
	Impeller radius max	64.8	cm	
	Blade height min	1.1	cm	
	Blade height max	4.3	cm	

	Blade length min	26.6	cm	
	Blade length max	48.7	cm	
	Max Mach number	0.51		
	CO2 temperature inlet	90.28	C	
	CO2 temperature outlet	184.2	C	
	CO2 pressure inlet	7.629	MPa	
	CO2 pressure outlet	19.96	MPa	
	CO2 flow rate	398.3	kg/s	
	Efficiency	87.8	%	Total-to-static
	CO2 mass	42.0	kg	Operating conditions

3. Multiple-Recompression Cycle

The current reference S-CO_2 cycle layout (Figure 2) – sometimes called a "recompression cycle" – was selected to compensate for the difference in the specific heats of the high and low pressure CO_2 flows in the low temperature recuperator (LTR). The difference in specific heats over the LTR temperature range for 7.4 MPa and 20 MPa is so significant (Figure 3) that the benefits from splitting the CO_2 flow to increase the LTR effectiveness overcome the drawbacks of the less efficient direct compression of a part of the uncooled CO_2 flow. As a result, the recompression Brayton cycle configuration provides a higher efficiency than the simple Brayton cycle configuration provided that an optimal flow split fraction is selected.

For the high temperature recuperator (HTR) temperature range, the difference in CO_2 specific heats is not so significant, as shown in Figure 3. For that reason, splitting the CO_2 flow to improve the effectiveness of HTR would not improve the cycle efficiency as much as it does for the LTR. Thus, only one flow split for the LTR is implemented in the reference cycle.

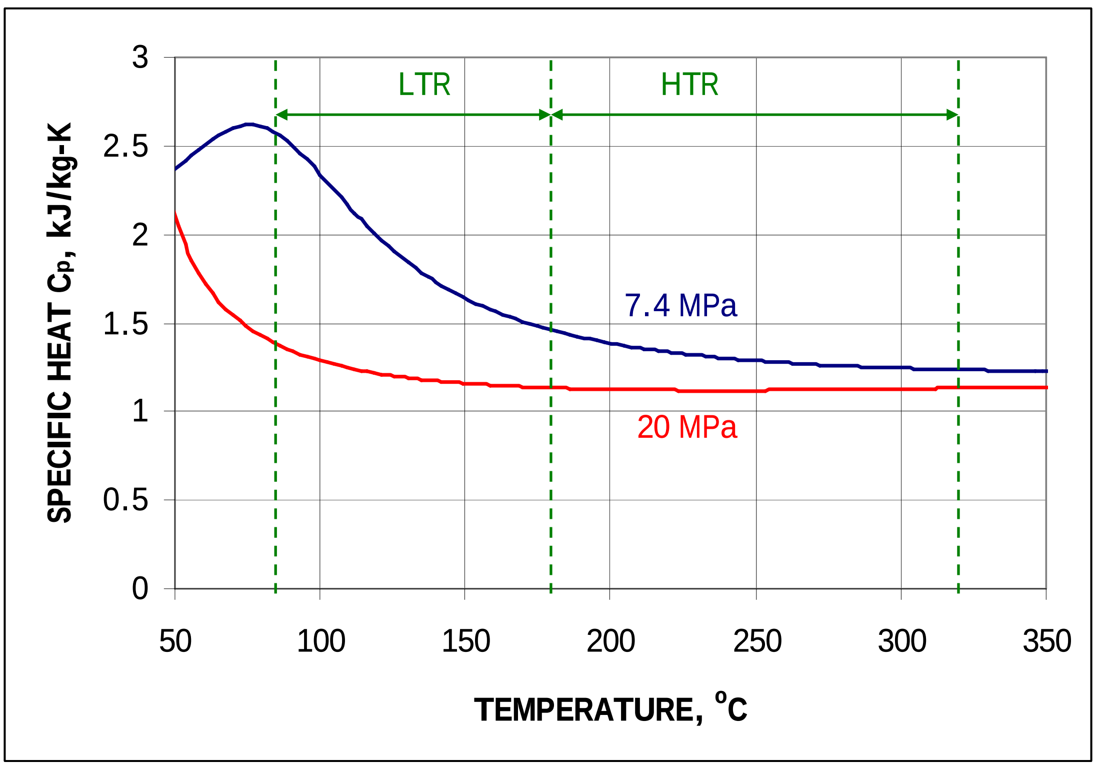

Figure 3. CO_2 Specific Heat Variation in Recuperators.

Even though the differences in the specific heats is not so large in the HTR temperature range (compared to the LTR temperature range), there is still a potential to improve the HTR effectiveness by employing a second CO_2 flow split involving the HTR. Similar to the recompression cycle, this flow split arrangement would result in the splitting the HTR heat exchanger into two serial units (the added recuperator is called a medium temperature recuperator or MTR) and adding an additional compressor. This arrangement is called a “double recompression” cycle in this report. If efficiency benefits for this arrangement are demonstrated, then more recompression loops could potentially be added resulting in “multiple recompression” cycles.

Figure 4 shows the performance of a double recompression cycle. Even though the temperature difference at the top of all recuperators has decreased to about 30 ^oC (compared to about 40 ^oC for the recompression cycle in Figure 2), the resulting cycle efficiency has actually decreased compared to that of the reference case. Two possible reasons can be identified to explain the reduction in the cycle efficiency. First, the benefits of the increased recuperator performance are offset by the compression of even hotter CO_2 in the second recompressing compressor. Second, as can be seen from Figure 2 and Figure 4, the CO_2 temperature at the Na-to-CO_2 HX inlet (HTR cold side outlet) is already close to the Na outlet temperature even at the reference conditions. Since the CO_2 temperature cannot exceed the Na temperature, any possible improvement in recuperator performance is limited by the sodium temperature. This is another specific feature of the S-CO_2 cycle for a SFR. When applied to other types of reactors which have higher reactor side temperatures (e.g., the High Temperature Gas-Cooled Reactor), the benefits of the double-recompression cycle configuration considered here could be more significant, if the recuperator performance is not limited by the heat addition temperatures. On the other hand, even for SFR temperatures, the fact that the cycle performance is limited not only by the turbine inlet temperature but also by the low end of the heat addition temperature range, may present an opportunity to improve the whole plant performance by optimizing the reactor side lower temperature. As noted above, though, optimization of the reactor system temperatures is beyond the scope of the current work. Based on the results obtained here, it is believed that the benefits from such an optimization would be more significant for the double recompression cycle compared to the single recompression cycle.

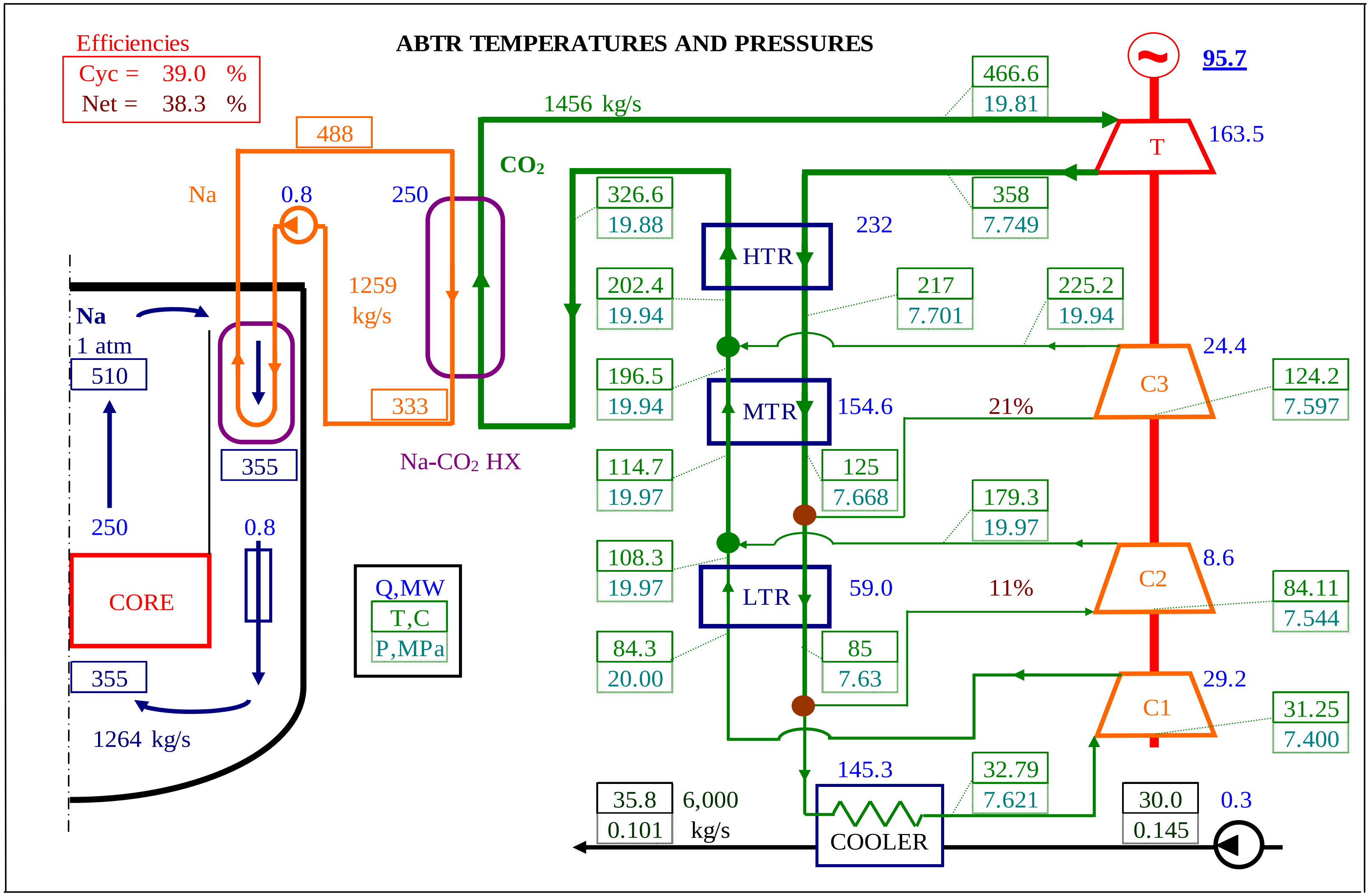

Figure 4. Double-Recompression S-CO_2 Cycle Layout and Calculated Performance.

4. Cycle Operating Conditions

In this chapter, the cycle operating conditions – temperatures and pressures – are varied to determine the conditions that provide the highest cycle efficiency. Previously, the reference cycle conditions (Figure 2) were selected such that the minimum pressure and temperature were set close to but still above the critical point. The maximum pressure was selected as 20 MPa based on the fact that beyond this pressure, the gain in cycle efficiency diminishes [4]. However, previous analysis has never been applied to the "low" temperature S-CO_2 cycle design for a SFR. The selection of the operating parameters is revisited in this chapter. In addition to simple parameter optimization, different cycle operating conditions, such as CO_2 condensation have been analyzed.

Among the cycle operating parameters, only the maximum CO_2 temperature is somewhat fixed by the reactor (sodium) side. The cycle efficiency increases with the maximum (turbine inlet) temperature (Figure 1), so it is beneficial to raise the CO_2 temperature in the Na-to-CO_2 heat exchanger as close to the Na temperature as is practically achievable.

For the recompression S-CO_2 Brayton cycle, the cycle efficiency depends on the CO_2 flow split between the compressors. Therefore, in the optimization presented below, each considered parameter is varied simultaneously with the flow split fraction; i.e., the fraction of the CO_2 flow which goes through the cooler and the main compressor, to insure that the optimal operating conditions are maintained during the main parameter variation.

4.1. Maximum Pressure

Figure 5 shows the dependency of the cycle efficiency on the maximum CO_2 pressure. In the analysis, the size of each piece of equipment is fixed, including the number of stages for the turbine and compressors. Figure 5 generally confirms that very little gain in cycle efficiency could be realized by raising the maximum cycle pressure above 20 MPa. Raising the pressure would require greater thicknesses for the piping, pressure-bearing casings, and heat exchangers resulting in higher capital costs. Still, about a 0.3 % increase in cycle efficiency can be achieved if the maximum cycle pressure is raised to 22 MPa. Again, this number represents the efficiency benefit for the equipment optimized previously for 20 MPa conditions. Further increase in efficiency could potentially be achieved through optimization of the turbomachinery and heat exchangers for the greater pressure.

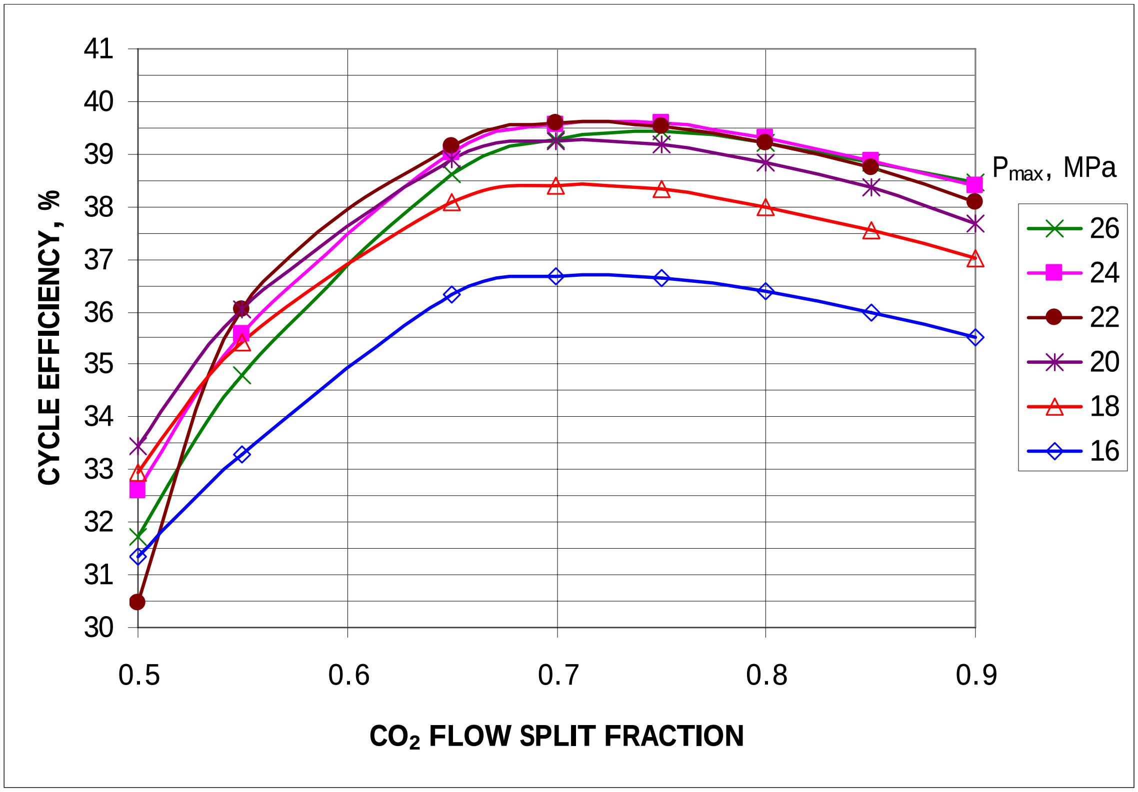

Figure 5. Optimization of Maximum CO_2 Pressure.

4.2. Minimum Cycle Temperature and Pressure

Depending on the temperature and pressure of the CO_2 flow at the main compressor inlet, the CO_2 conditions could vary from supercritical to supercritical/subcritical liquid, supercritical/subcritical gas, and liquid-gas (two-phase) mixture. Figure 6 defines the CO_2 conditions near the critical point as they are referenced in this document. Consequently, the name of the cycle corresponds to the CO_2 conditions at the main compressor inlet; i.e., if CO_2 enters the main compressor at supercritical conditions, the cycle is called "supercritical." Cycles in which CO_2 enters the compressor in a two-phase region are not considered for this work. If the CO_2 goes through the two-phase region before it enters the compressor, the cycle is called a "condensation" cycle.

Appendix A shows T-s and h-s diagrams for carbon dioxide for the range of the cycle operating conditions with greater detail near the CO_2 critical point.

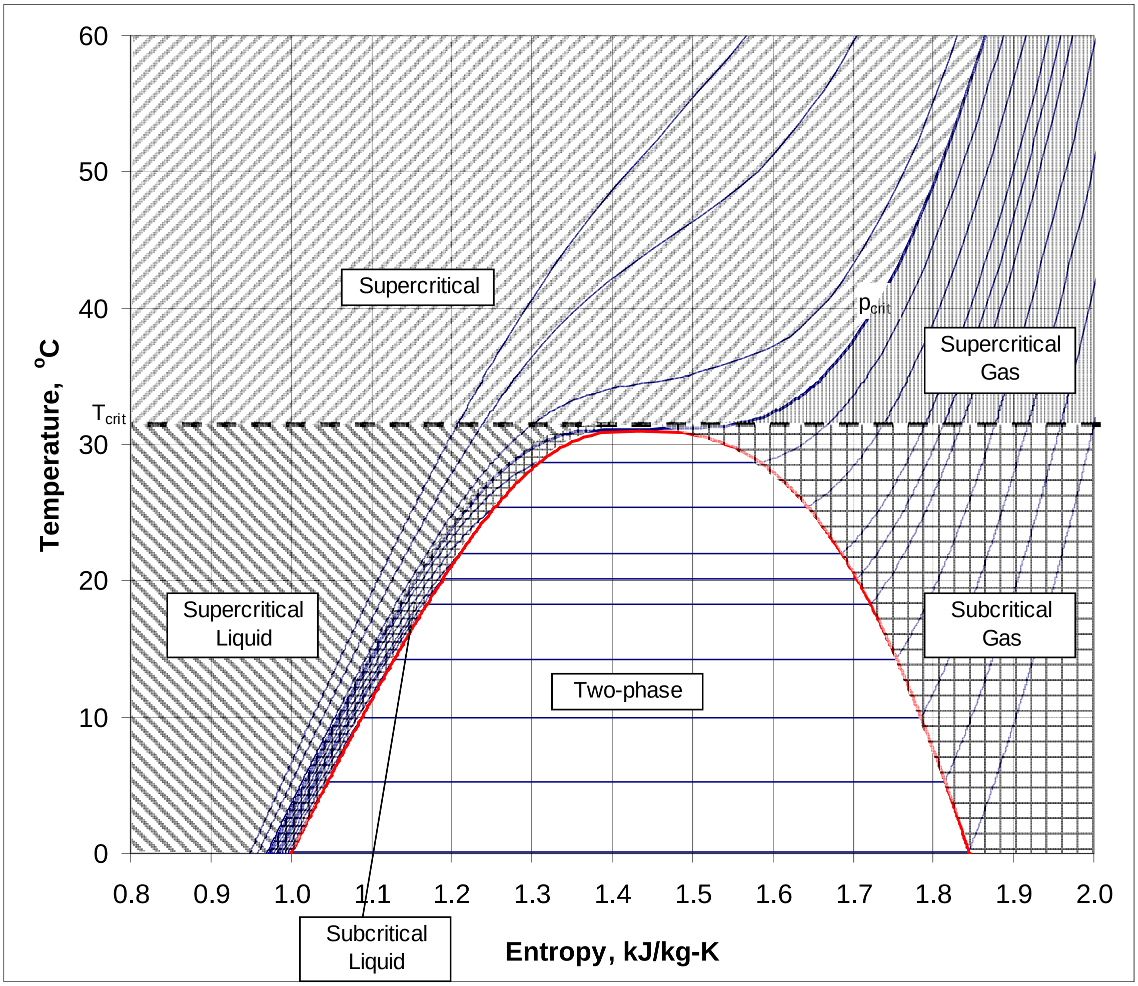

Figure 6. CO_2 Conditions near the Critical Point.

Figure 7 shows the tradeoff between the cycle efficiency and the required cooler volume based on which the reference conditions (Figure 2) selected for the ABTR S-CO_2 cycle. The results in Figure 7 were obtained for the fixed minimum pressure of 7.4 MPa. Since the selected pressure is above the critical value while the temperature is below the critical temperature, Figure 7 effectively compares the supercritical cycle with a cycle in which CO_2 enters the main compressor in a liquid phase at supercritical pressure. Even though the liquid phase cycle operating at supercritical pressure results in a higher efficiency, in order to cool CO_2 below the critical temperature (or, more accurately, the pseudocritical temperature for the selected pressure), the CO_2 flow has to pass through the peak in the specific heat resulting in a requirement for a significant increase in the cooler heat transfer area. Thus, the temperature just above the pseudocritical value, 31.25 °C, was selected for the reference ABTR conditions. For this study, however, the cooler volume is not an important consideration so that conditions even more different from the reference case than those shown in Figure 7 are investigated, as presented below.

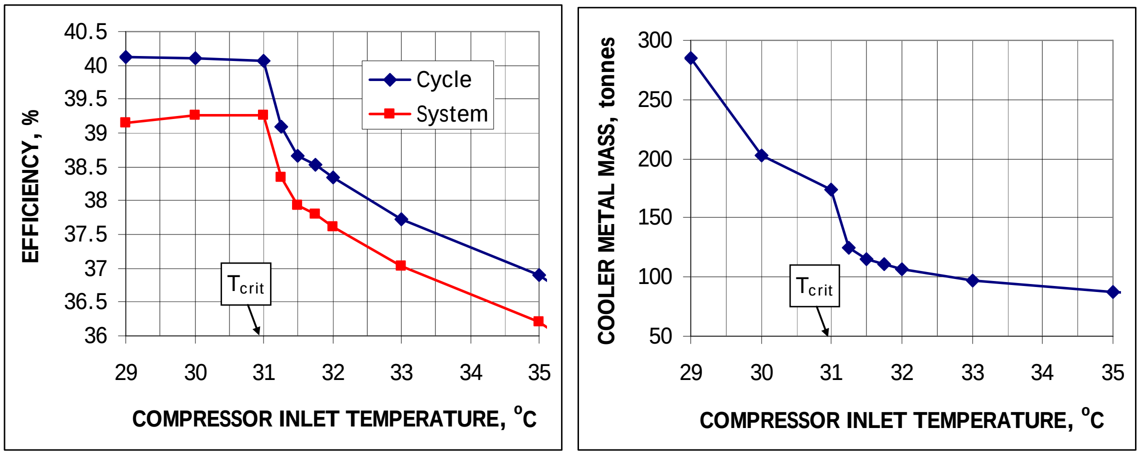

Figure 7. CO_2 Cycle Efficiency versus Minimum Temperature and Cooler Volume Tradeoff. [8]

4.2.1. Minimum Temperature with Supercritical Pressure – Supercritical Cycle versus Liquid at Supercritical Pressure Cycle

Figure 8 shows in greater detail how the cycle efficiency varies with the minimum temperature during the transition from supercritical to the liquid phase at supercritical pressure. As in Figure 7, the peak cycle efficiency is achieved at 30 °C. Cycle efficiency for the cases where the liquid CO_2 enters the main compressor (strictly speaking, a pump) in a liquid phase at temperatures slightly lower than the critical temperature (20-31 °C) is close to the peak efficiency. Both these facts are due to the high CO_2 density in the liquid phase at the compressor/pump inlet.

The results in Figure 7, as well as other results in this chapter, are obtained under the assumption that a cold heat sink is available to cool the CO_2 below 30 °C, if needed. The heat sink (water) temperature for the reference conditions is assumed to be at 30 °C, as shown in Figure 2.

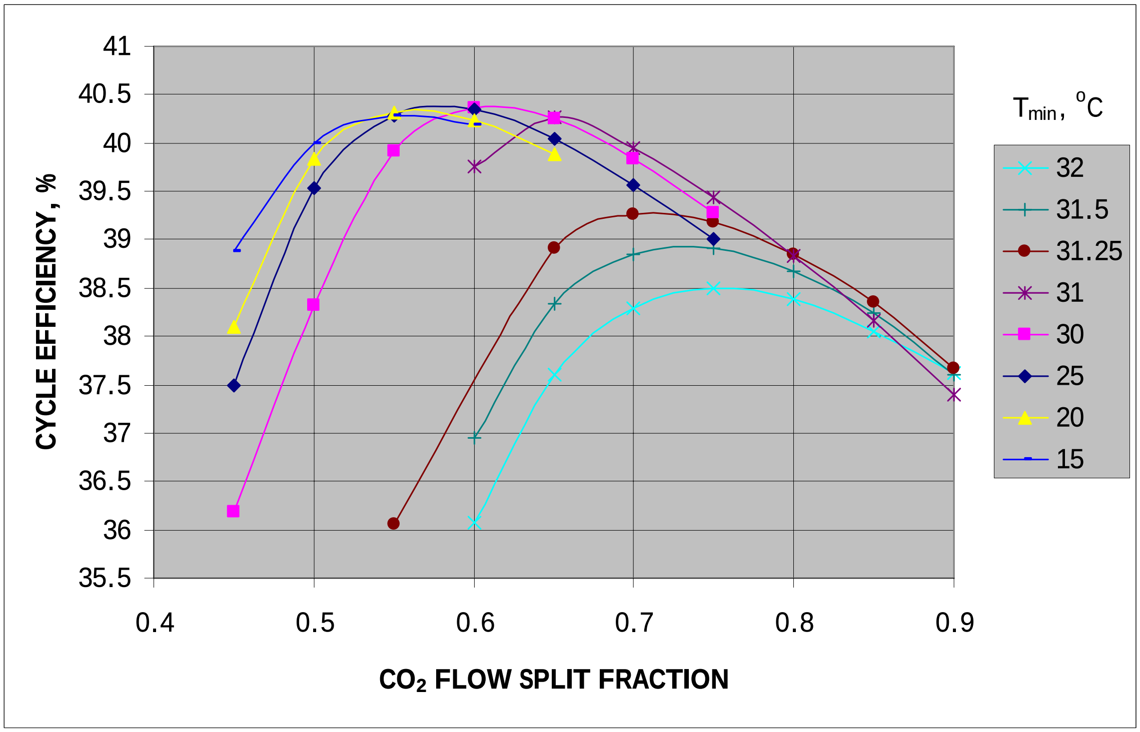

Figure 8. Effect of the Cycle Efficiency versus Minimum Temperature (p_{min}=7.4 MPa).

4.2.2. Minimum Pressure with Supercritical Temperature – Transition through a Pseudocritical Point in the Cooler

Figure 8 showed that greater cycle efficiency could be achieved if CO_2 is cooled below the pseudocritical temperature at the selected supercritical pressure. For pressures above the critical value, the pseudocritical temperature lies above the critical temperature. Similar results could be achieved by a variation of the minimum pressure at a fixed temperature. **Figure 9** demonstrates that the pseudocritical temperature (temperature at which a peak in specific heat occurs for a given pressure) increases with pressure. **Figure 9** also demonstrates that the density increases with pressure for a fixed temperature. For example, the density jumps sharply at 31.3 ^{o}C from 7.40 MPa to 7.45 MPa. This is due to the fact that the pseudocritical temperature is below 31.3 ^{o}C for 7.40 MPa and above that for 7.45 MPa. If, for a fixed temperature, the pressure is selected such that the compression occurs close to the pseudocritical conditions, the high CO_2 density would provide lower compressional work and, therefore, higher cycle efficiency. Similar to the previous cases, this benefit would come at the price of a larger cooler requirement since CO_2 would need to be cooled below the peak in the specific heat (i.e., a greater energy removal in the cooler).

Figure 10 shows the possibility to improve the cycle efficiency at the expense of the cooler volume by means of the minimum pressure variation at the reference minimum temperature. Figure 11 presents the same results with optimal flow split values selected at each pressure. Figure 12 and Figure 13 show that the effect is somewhat smoothed out for a slightly higher temperature of 31.5 ^{o}C versus 31.25 ^{o}C.

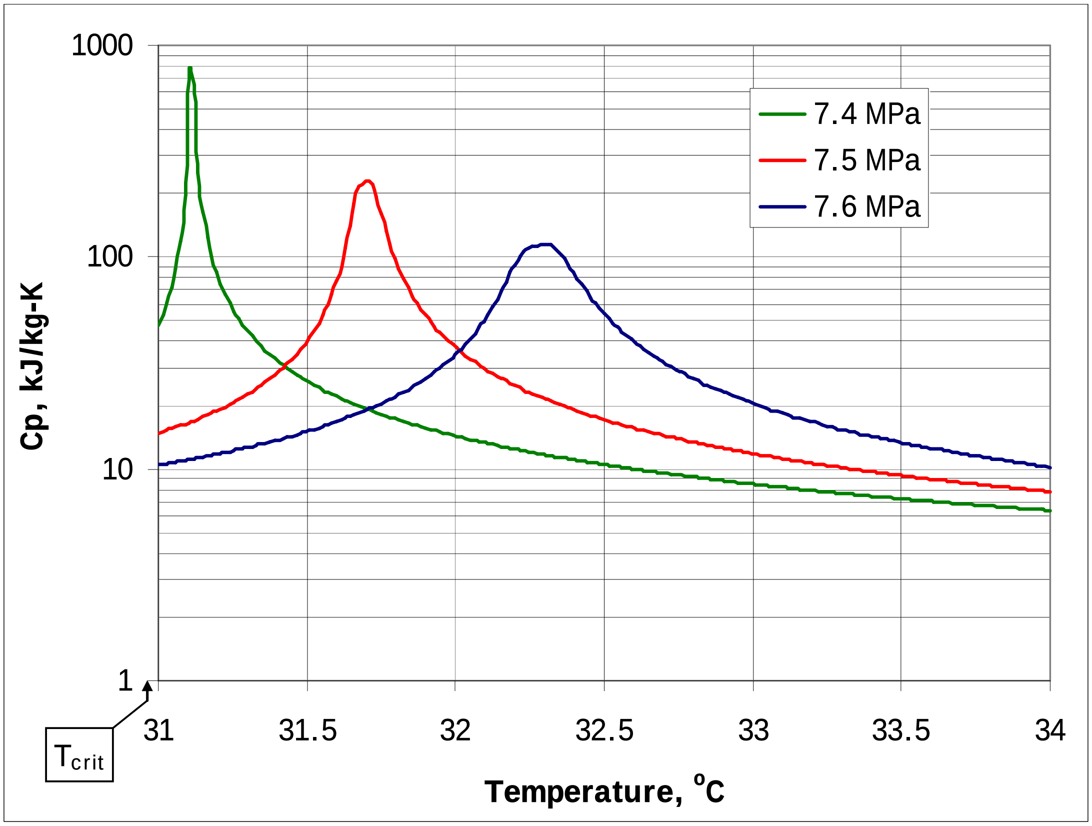

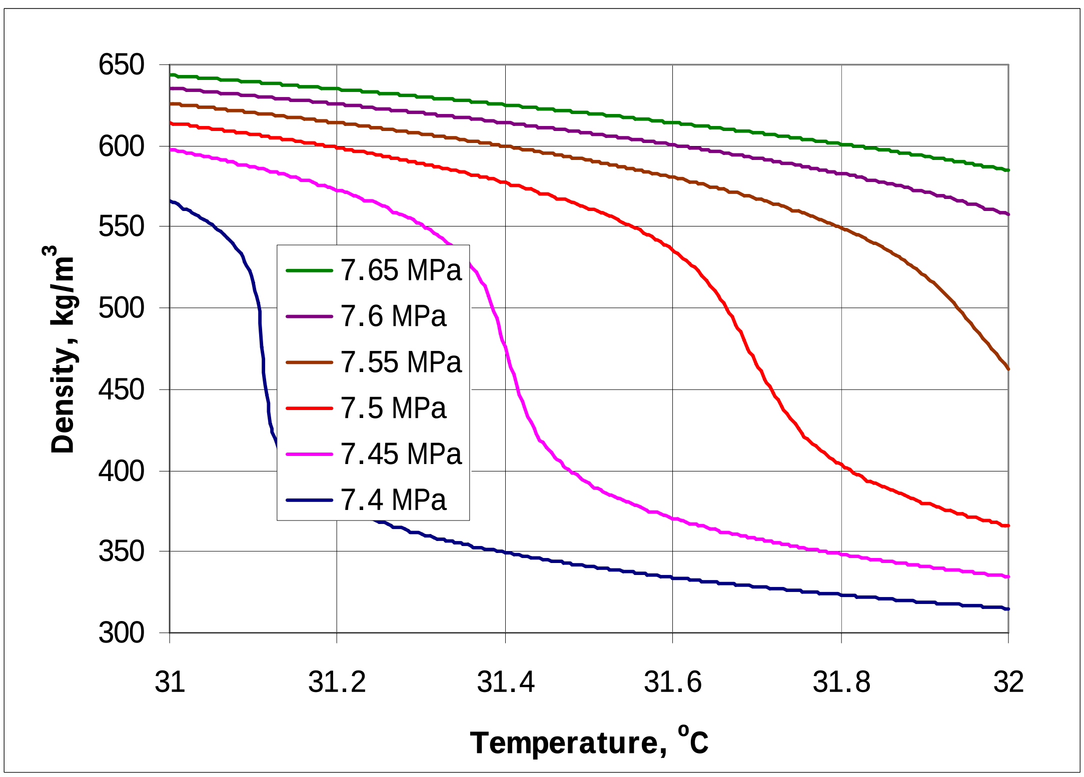

Figure 9. CO_2 Properties Variation near the Pseudocritical Points.

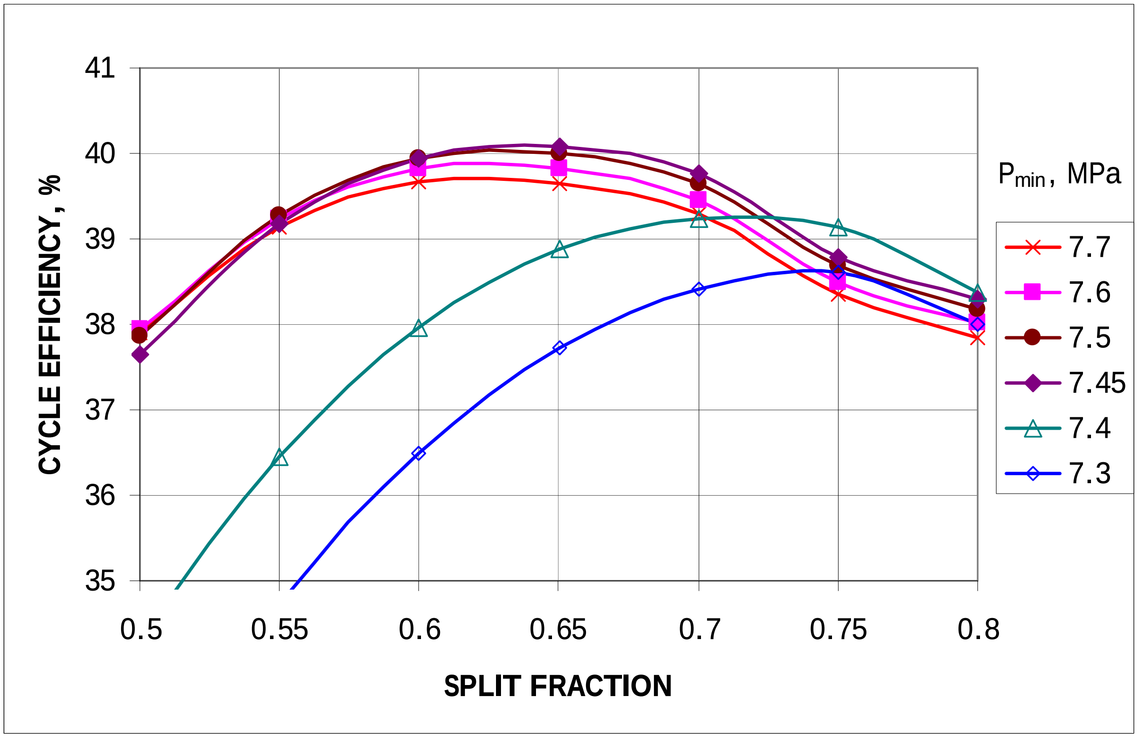

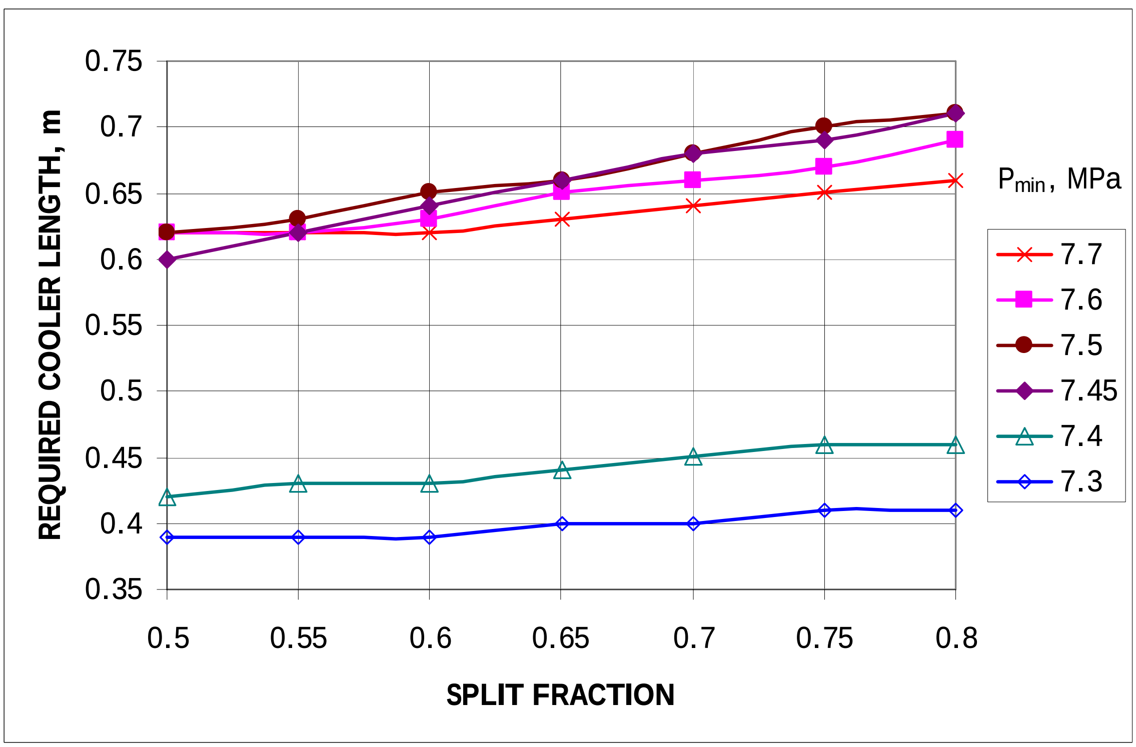

Figure 10. S-CO_2 Brayton Cycle Efficiency Dependency on Minimum Pressure with Supercritical Temperature (T_{min}=31.25 ^oC).

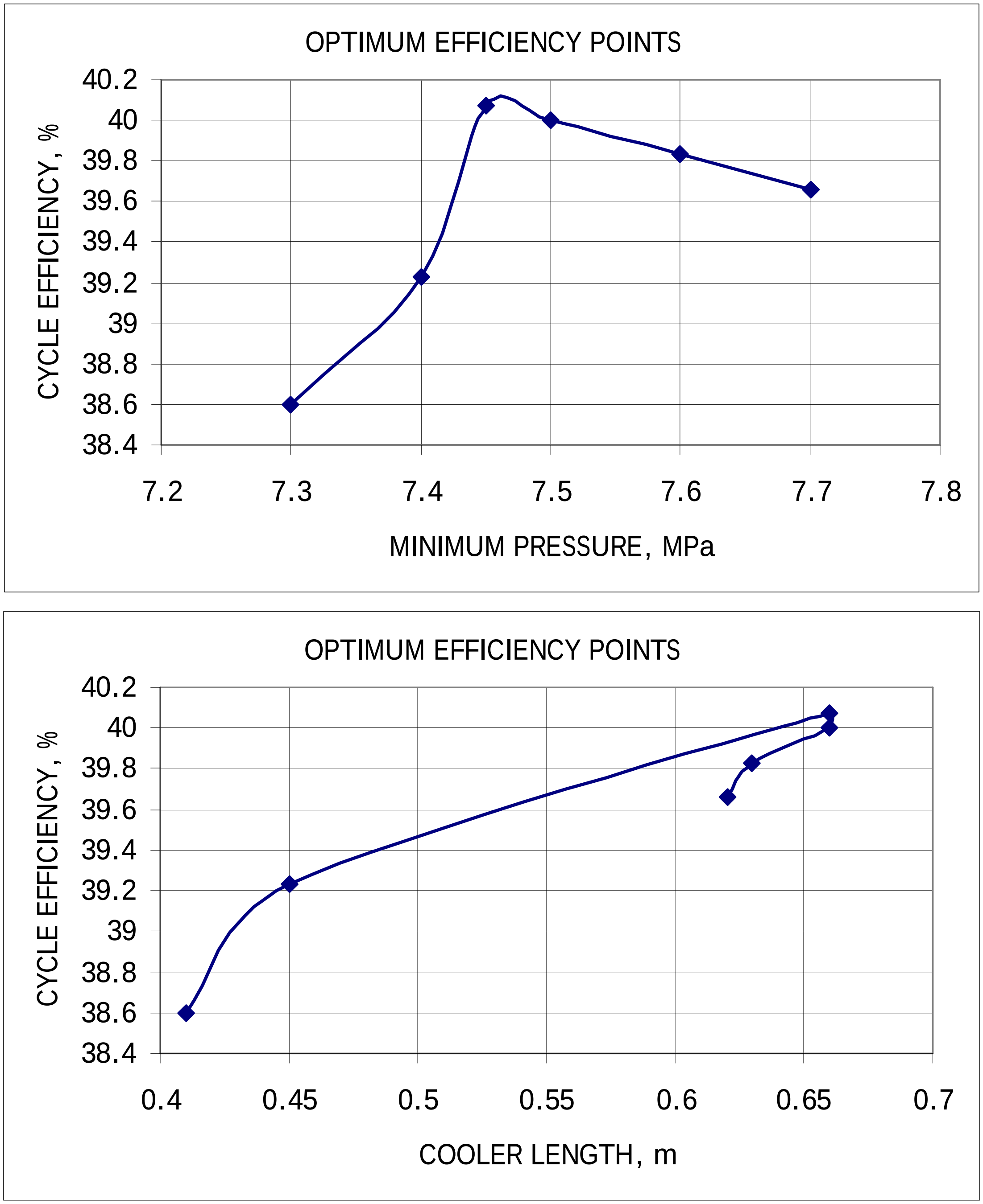

Figure 11. Trade-off between the Cycle Efficiency and Cooler Volume with Minimum Cycle Pressure (Optimum Flow Split Points, T_{min}=31.25 ^oC).

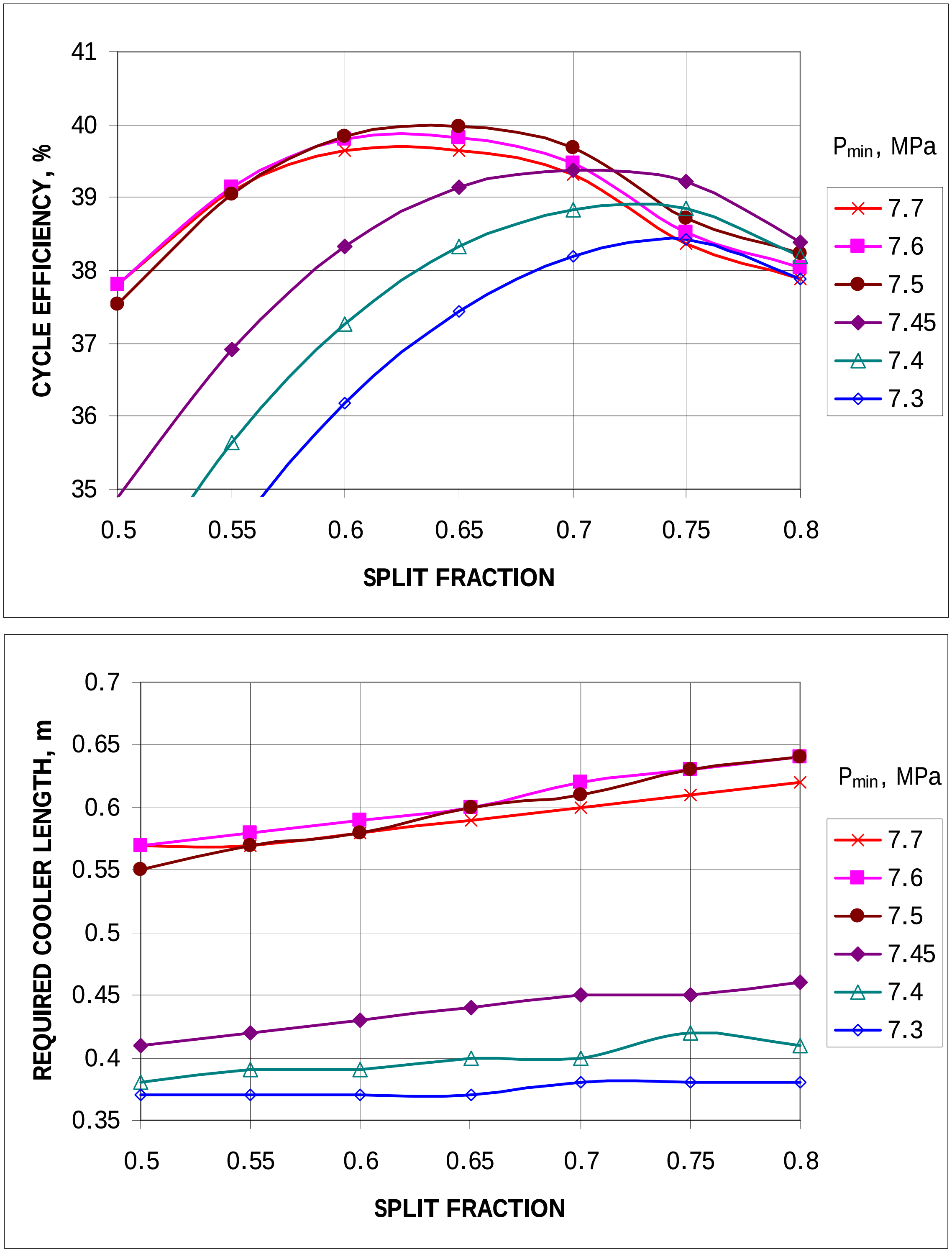

Figure 12. S-CO_2 Brayton Cycle Efficiency Dependency on Minimum Pressure with Supercritical Temperature (T_{min}=31.50 ^oC).

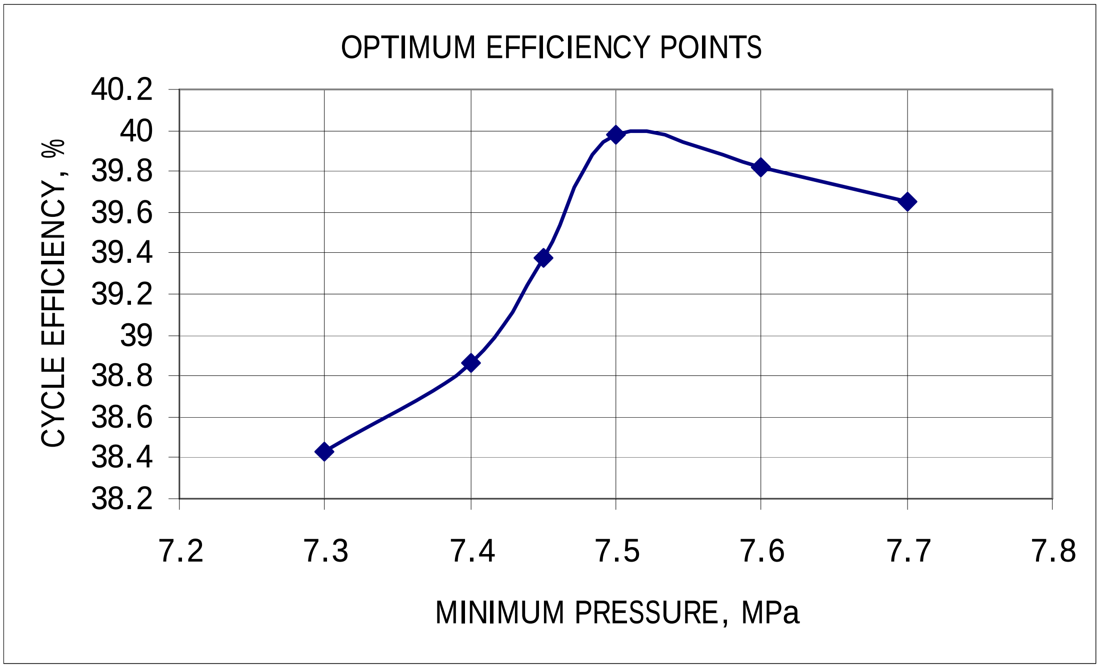

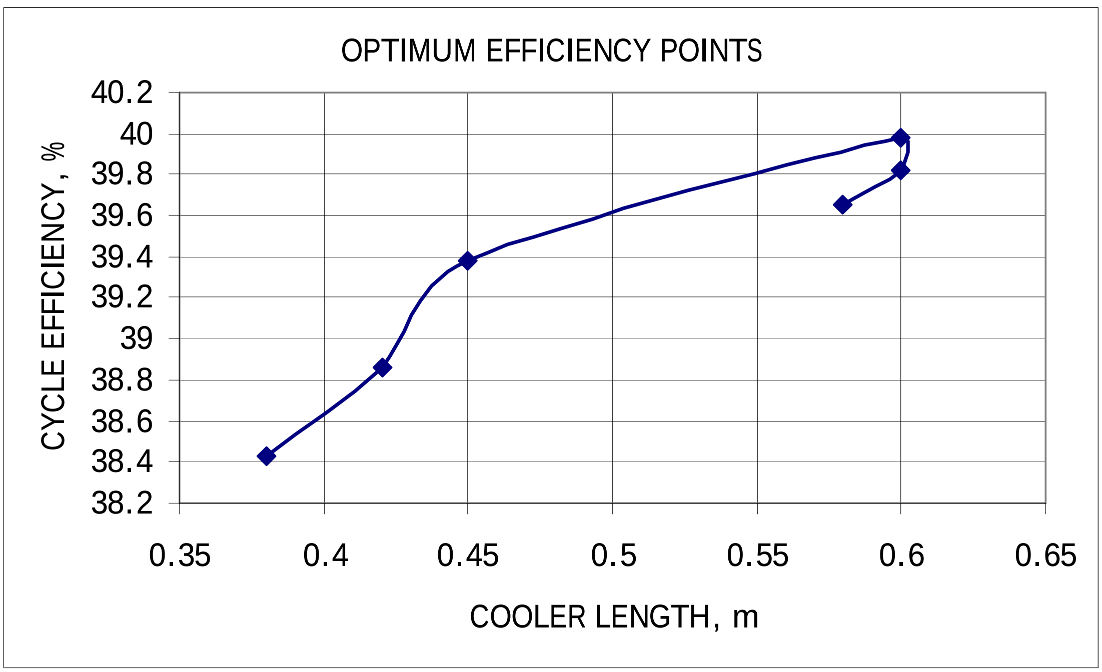

Figure 13. Tradeoff Between the Cycle Efficiency and Cooler Volume with Minimum Cycle Pressure (Optimum Flow Split Points, T_{min}=31.50 ^oC).

4.2.3. CO_2 Cycle with Minimum Temperature Below the Critical Value

The results shown above (Figure 8) demonstrate the cycle efficiency benefits if CO_2 is cooled below its critical temperature while supercritical pressure is maintained. The operation of the subcritical cycle is expected to be significantly different from that of a supercritical cycle such that the effect of the operating pressures, both high and low, are reinvestigated here for subcritical temperature.

Figure 14 shows how the cycle efficiency depends on the minimum pressure if CO_2 is cooled down to 20 ^oC. It follows from Figure 14 that the peak efficiency is achieved when the minimum pressure equals to the saturation pressure (5.75 MPa for 20 ^oC, see Appendix A). Under these conditions, CO_2 expands in the turbine from supercritical to subcritical pressures, then it is cooled to a subcritical vapor and is condensed in the cooler (strictly speaking, a condenser in this case) down to saturated liquid conditions (Figure 6). This cycle is similar to the traditional supercritical water cycle. Figure 14 shows, however, that there still exists an optimal flow split such that a recompression cycle configuration is beneficial for this CO_2 cycle. It is noted that the calculations for Figure 14 are carried out with the same model developed for the supercritical cycle such that realistic cooler/condenser calculations are not possible by the current single-phase model. Instead, some value for the condenser pressure drop on CO_2 side, 1 %, is simply assumed in the calculations (compared to 0.03 % calculated for the reference cooler conditions). Condenser sizing calculations are not carried out.

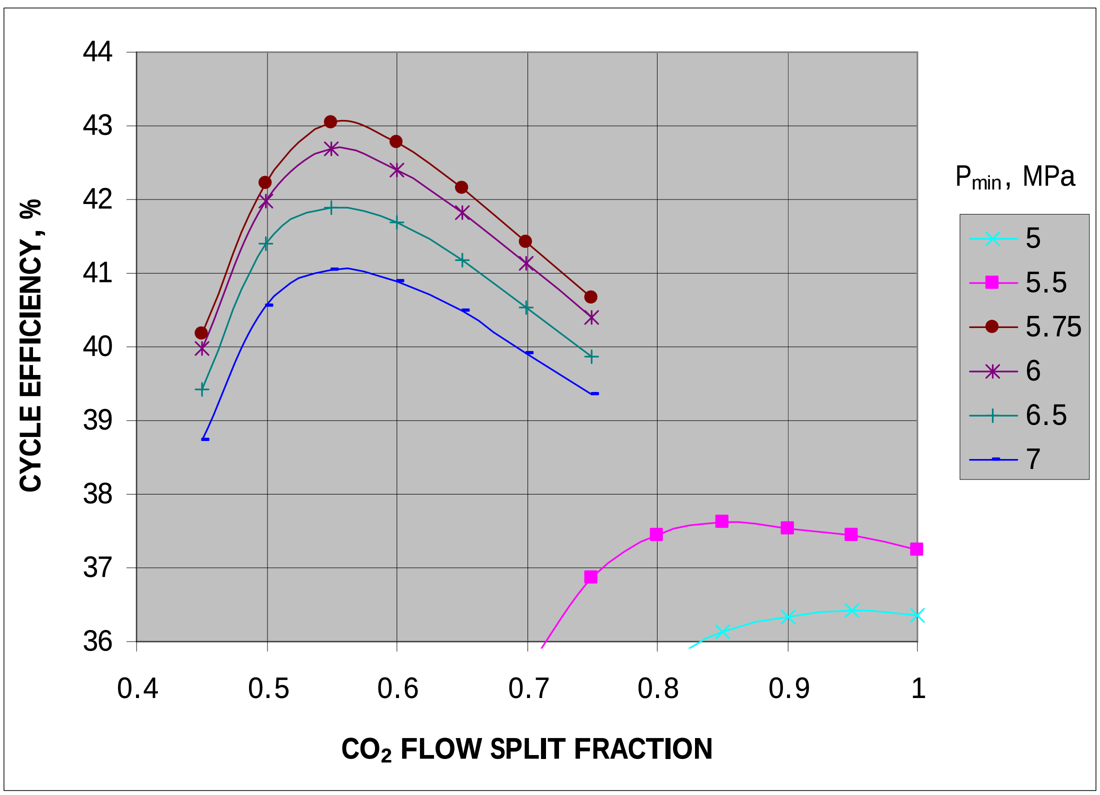

Figure 14. CO_2 Cycle Efficiency versus Minimum Pressure for Subcritical Minimum Temperature (T_{min}=20 ^oC).

The results in Figure 14 show that the maximum cycle efficiency is achieved at the saturation pressure. If the pressure is selected above that value, then CO_2 is cooled in the liquid phase below its saturation point. Figure 14 demonstrates that such operation yields lower cycle efficiency. Operation with the pressure below the saturation pressure simply transforms the cycle into a simple gas Brayton cycle where CO_2 is compressed in the (subcritical) gas phase. The efficiency of such a cycle is significantly lower than that of the condensation cycle, as shown in Figure 14.

Figure 15 shows the dependency of the condensation cycle efficiency on the maximum pressure. The results are similar to those obtained previously for the supercritical cycle – the increase in cycle efficiency above 20 MPa is minimal. Again, the results presented here are obtained under the assumption of fixed equipment. Optimization of the equipment for these operating conditions would be expected to improve the cycle efficiency.

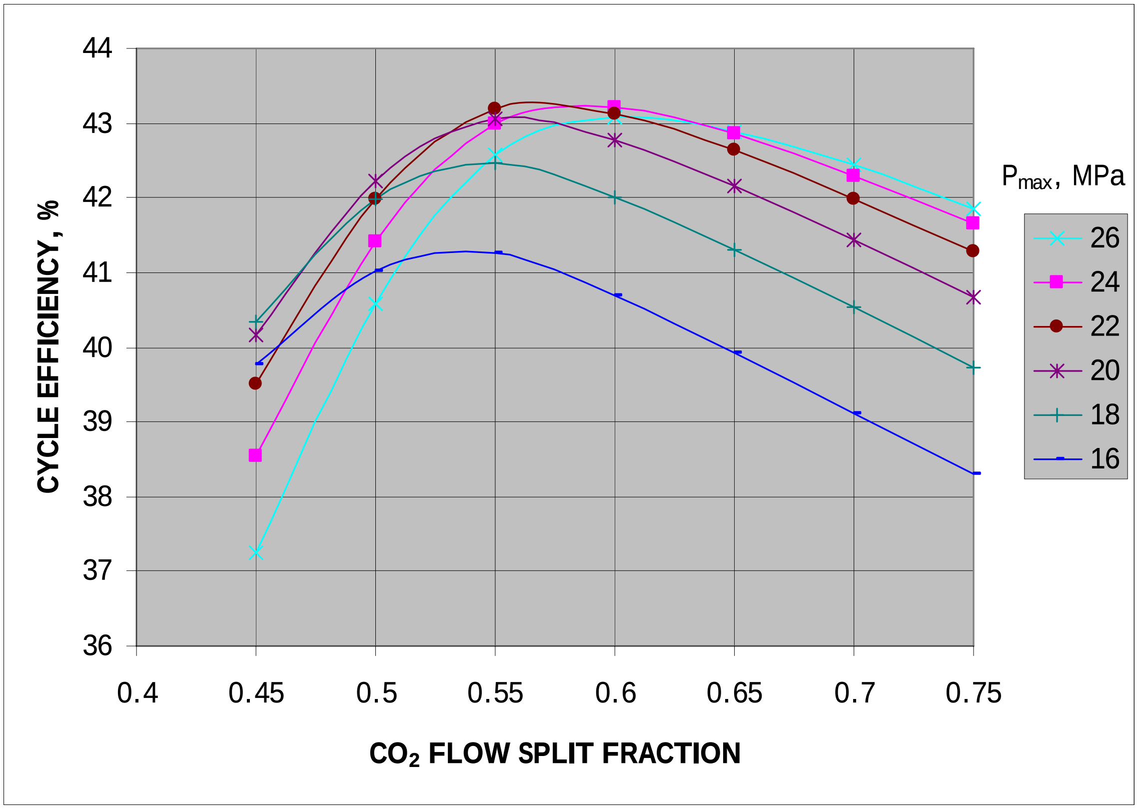

Figure 15. Optimization of Maximum Pressure for Condensation Cycle (T_{min}=20 ^oC, p_{min}=5.75 MPa).

Figure 16 shows the conditions and performance of the condensation CO_2 cycle. An efficiency of 43 % (up from 39 % in reference case) is calculated for SFR reactor temperature conditions, provided that a heat sink temperature below 20 ^oC is available.

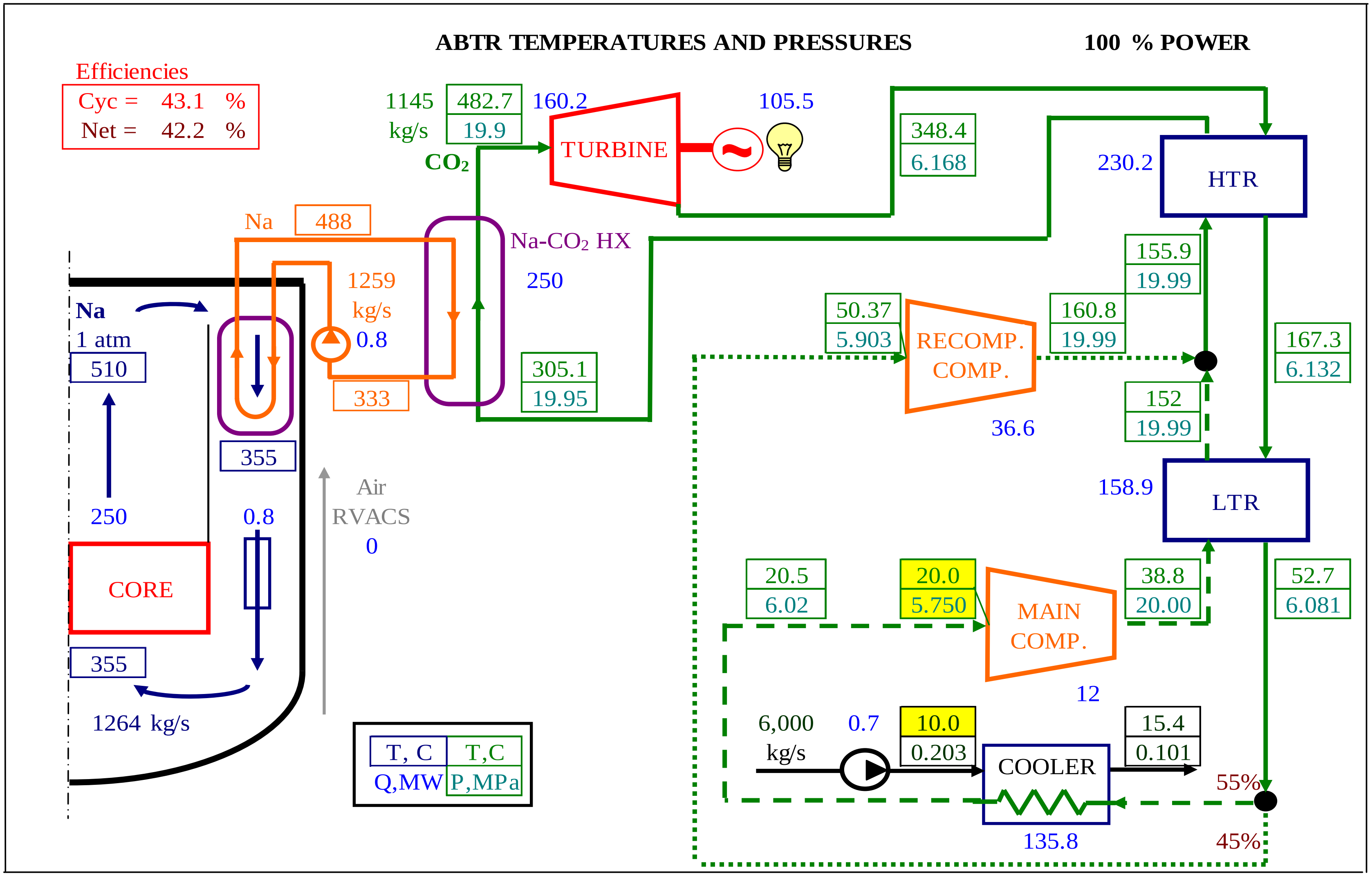

Figure 16. CO_2 Condensation Cycle Performance and Conditions.

5. Cycle with Intercooling

An intercooling cycle configuration, in which a compressor is split into two stages with working fluid cooling between the stages, is frequently used for ideal gas Brayton cycles to reduce the overall compressional work and, therefore, increase the cycle efficiency. In the S-CO_2 cycle, however, the compressional work is already small such that the benefits from the intercooling are also expected to be small. In addition, intercooling between the compressor stages reduces the temperature at the compressor outlet (recuperator inlet) such that the performance of the recuperators is expected to be affected, especially for the low temperature recuperator where the proximity to the critical point affects the performance significantly.

The S-CO_2 cycle developed at the Tokyo Institute of Technology is based on a minimum CO_2 temperature of 35 ^oC, a low end pressure of 7.1 MPa that is subcritical, and utilizes intercooling between two main compressors instead of a single main compressor [7].

Figure 17 shows the cycle configuration, parameters, and performance of the S-CO_2 Brayton cycle with intercooling between the main compressor stages. The intercooling pressure is selected such that the pressure ratios of the two stages of the compressor would be about the same. It is assumed that as a result of intercooling the CO_2 reaches the same temperature at the second compression stage inlet as for the first stage, 31.25 ^oC. The CO_2 flow split fraction between the main and the recompression compressors is selected to optimize the cycle efficiency.

Figure 17 demonstrates that the cycle efficiency for the intercooling cycle is slightly lower than that for the reference cycle. Therefore, no benefits could be achieved by implementing the intercooling between the main compressor stages. Similar calculations show that the intercooling between the recompression compressor stages does not improve the cycle efficiency either.

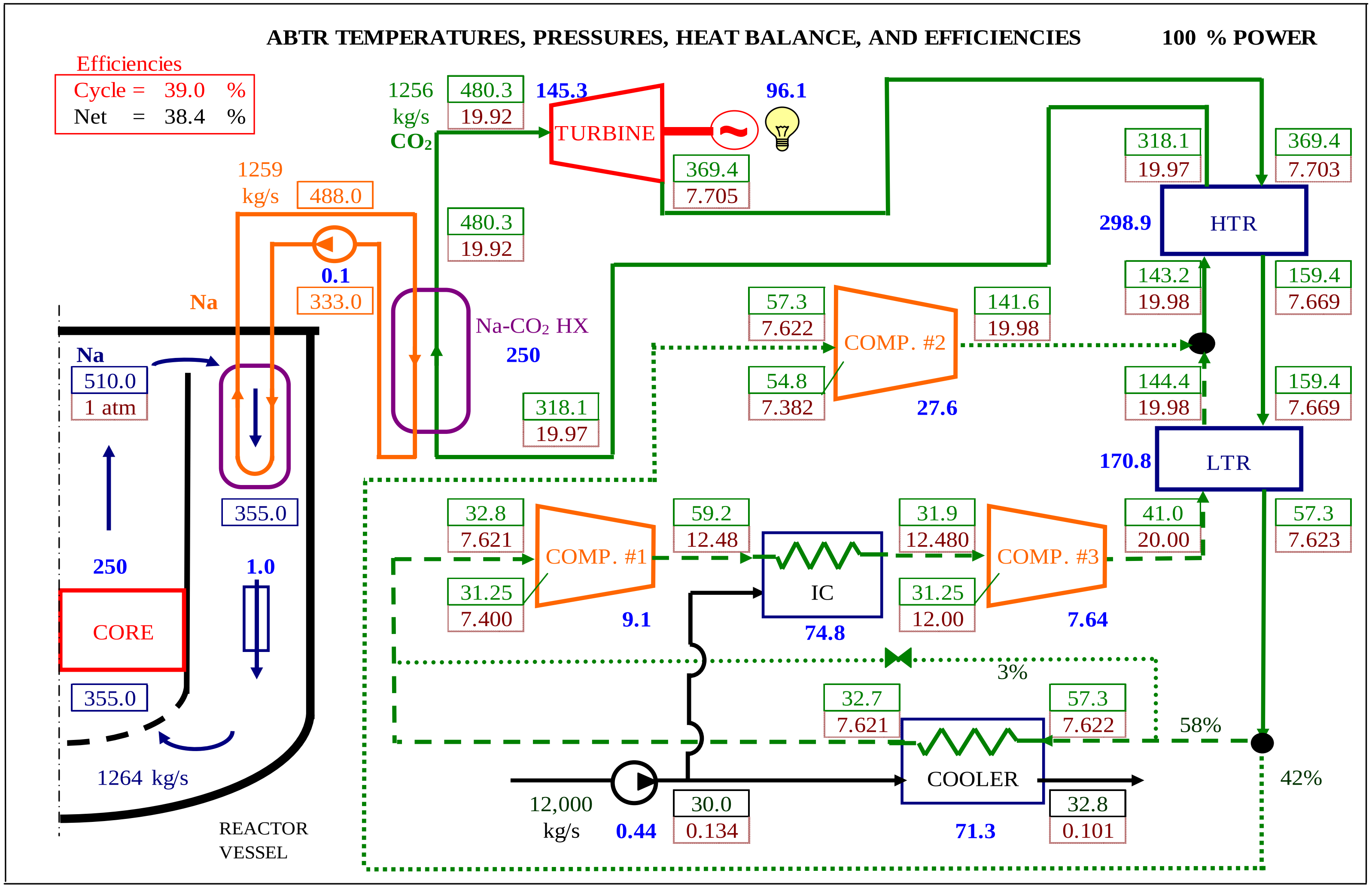

Figure 17. Configuration and Performance of the S-CO_2 Cycle with a Intercooling.

6. Cycle with Reheating

Reheating of the working fluid between the turbine stages is another common approach to improve the cycle efficiency for ideal gas Brayton cycles. It is also used for steam cycles. To investigate the effect of reheating on S-CO_2 Brayton cycle performance, an additional heat exchanger (reheater) and an additional turbine (low pressure turbine, LPT) are introduced into the cycle. CO_2 is still heated in the Na-to-CO_2 heat exchanger and expands in the turbine, but then, instead of being sent to the recuperator, it is reheated in another Na-to-CO_2 heat exchanger (reheater) and goes through the LPT before returning to a recuperator. It is assumed in this analysis that the CO_2 is reheated by intermediate sodium; thus, the sodium flow is split after the IHX between the main Na-to-CO_2 HX and the reheater.

Figure 18 shows the plant configuration, cycle conditions, and performance for the S-CO_2 cycle with a reheat. A 50/50 flow split is assumed for the sodium between the Na-to-CO_2 heat exchangers. The CO_2 pressure between the turbines is selected such that the pressure ratios for both turbines are about the same. Figure 18 demonstrates that the cycle efficiency is reduced compared to the reference case (Figure 2). Two possible reasons may be identified for the efficiency reduction. First, in the reference cycle configuration the temperature change in the Na-to-CO_2 HX is about the same on the Na and CO_2 sides (as a result of close specific heats for Na and CO_2). When the Na flow rate in the Na-to-CO_2 HX is reduced due to a Na flow split between the two heat exchangers, the temperature change on the CO_2 side is reduced in order to maintain a heat balance. As a result, CO_2 is heated up to a much lower temperature compared to the reference case (400 ^oC vs. 470 ^oC). For the same reasons, CO_2 heatup in the reheater is not very effective as well – CO_2 is reheated to only 415 ^oC. The other reason for the efficiency loss, although to a lesser degree, is doubling of the turbine exit losses for the two turbines in a serial configuration. CO_2 flow speed has to be reduced after the HPT to enter the reheater then the CO_2 flow has to be accelerated again to the LPT design speed.

Although Figure 18 shows the results of the 50/50 flow split for the intermediate sodium, an attempt to optimize this flow split failed since the cycle efficiency increases with the flow fraction to the main Na-to-CO_2 HX such that the most optimal configuration would be with 0 % flow to the reheater; i.e., for the cycle configuration without a reheat.

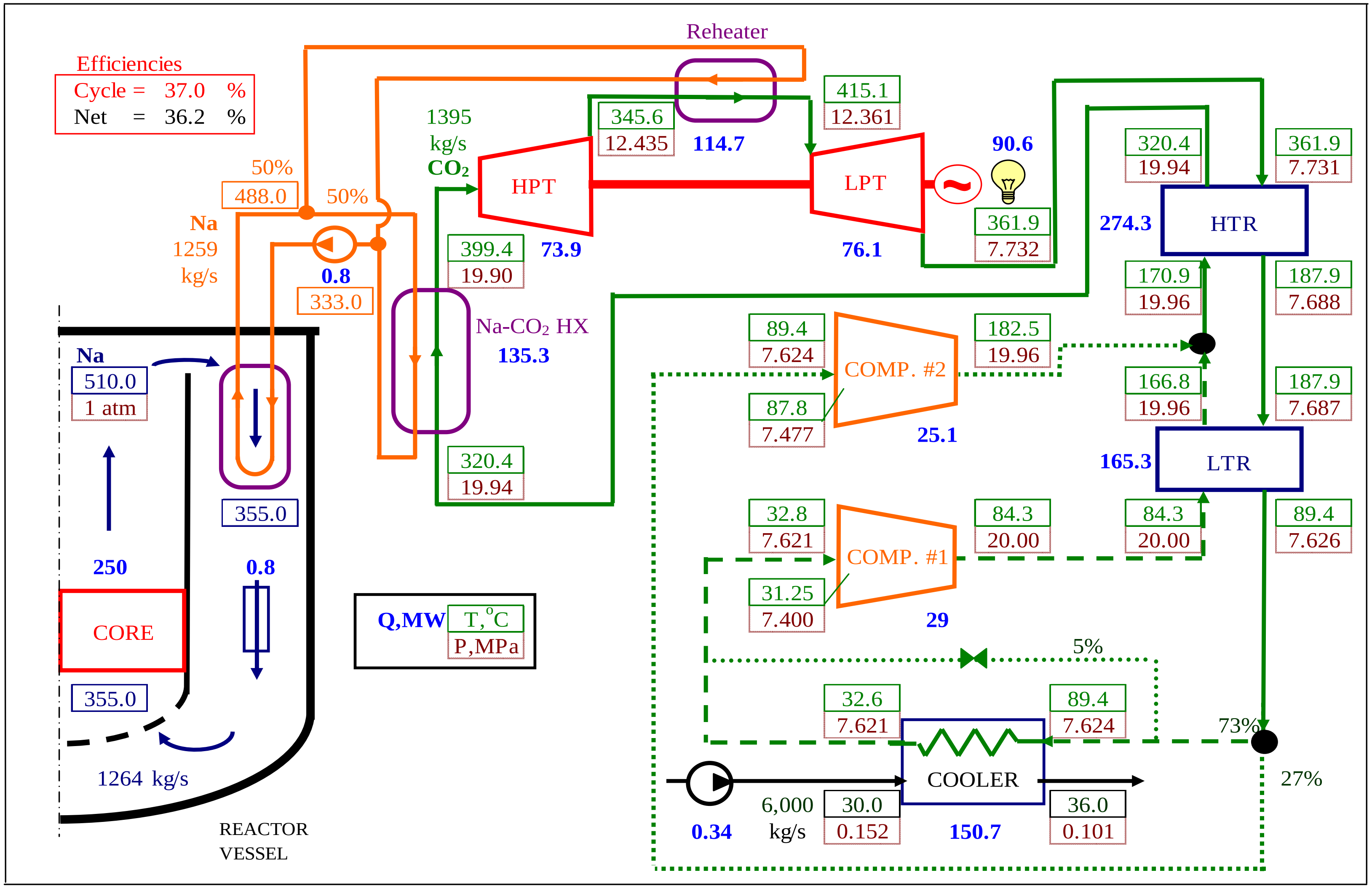

Figure 18. Configuration and Performance of the S-CO_2 Cycle with Reheating.

7. Component Size and Optimization

In previous analyses, the S-CO_2 cycle components such as heat exchangers and turbomachinery were designed to achieve reasonable performance at a reasonable cost (size). The exact meaning of what "reasonable" performance or cost means is not clearly defined; the components size selection has been carried out according to engineering judgment based on a tradeoff between the component size/performance and the benefits to the cycle performance. No detailed cost analysis for the entire cycle has yet been developed and applied to the size selection for each component.

Figure 19 shows how the size of the heat exchangers for the ABTR [8] has been selected. The size of each heat exchanger was selected at the point beyond which a return for the cycle efficiency starts to diminish with further increase in component size. Still, as it follows from Figure 19, there is a clear potential to increase the cycle efficiency beyond the reference value by selecting the heat exchangers to be larger that those assumed for the reference case. Figure 20 demonstrates a similar dependency of the ABTR cycle efficiency on the number of turbine stages. Similar to the heat exchangers, some gain in the cycle performance could be realized with a larger than reference turbine.

To determine the potential gain in cycle efficiency from component size increase, the S-CO_2 cycle performance has been calculated with larger components to compare to the reference case. First, to investigate how much efficiency is lost due to heat exchanger non-ideal performance, the cycle performance is calculated assuming "ideal" heat exchangers, i.e. heat exchangers with infinite heat transfer area and zero pressure drops. To model the "ideal" heat exchangers, the cross-sectional area (volume) of each heat exchanger is simply increased ten times. Figure 21 demonstrates that about a 3 % efficiency gain can theoretically be realized with larger heat exchangers. In addition to that, doubling the number of stages for the turbine (Figure 22) can add another 0.7 % efficiency resulting in total efficiency gain of up to 4 % from larger components. (An attempt to increase the cycle efficiency by implementing more compressor stages has not been carried out here since the previous analysis [8] demonstrates that the compressor operating near the critical point has a narrower design parameter selection range than the turbine such that an increase in number of stages is not always beneficial for its performance and for the performance of the cycle.) Even though the above numbers are calculated for an unrealistic ten-time increase in heat exchanger volume and, therefore, are not practical, they still show that there is a potential to increase the cycle efficiency beyond the reference case value. For example, calculations with twice the heat exchanger volume show that the cycle efficiency can be increased by about 1.5 %.

Figure 23 shows how the performance of the condensation cycle (Figure 16) can be increased by about 2 % by implementing heat exchangers and a turbine which are twice the size of the original (reference) case. The calculated efficiency, about 45 %, is the highest efficiency calculated so far for the CO_2 cycle for the assumed SFR temperature range.

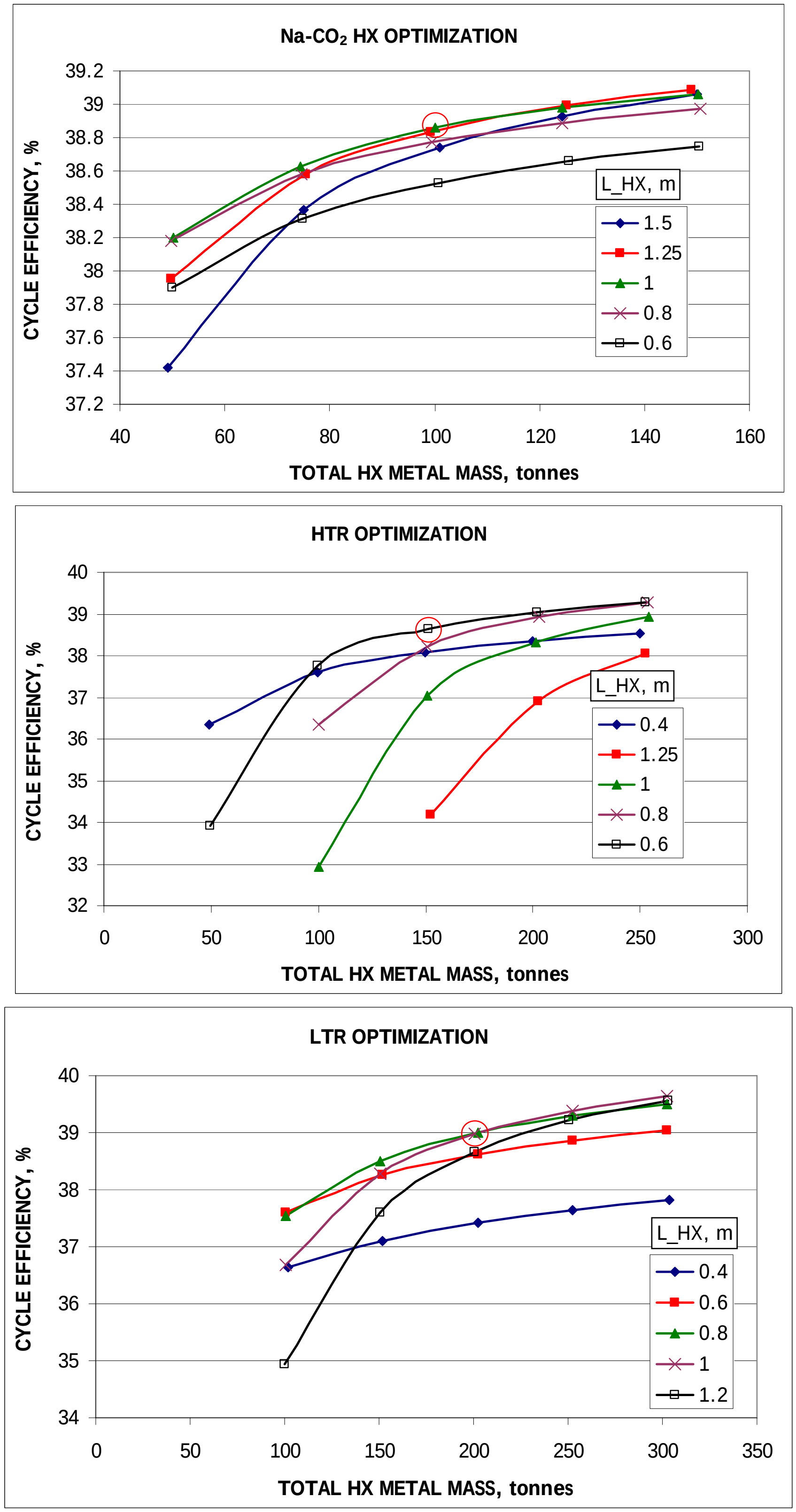

Figure 19. Heat Exchanger Optimization for the ABTR. [8]

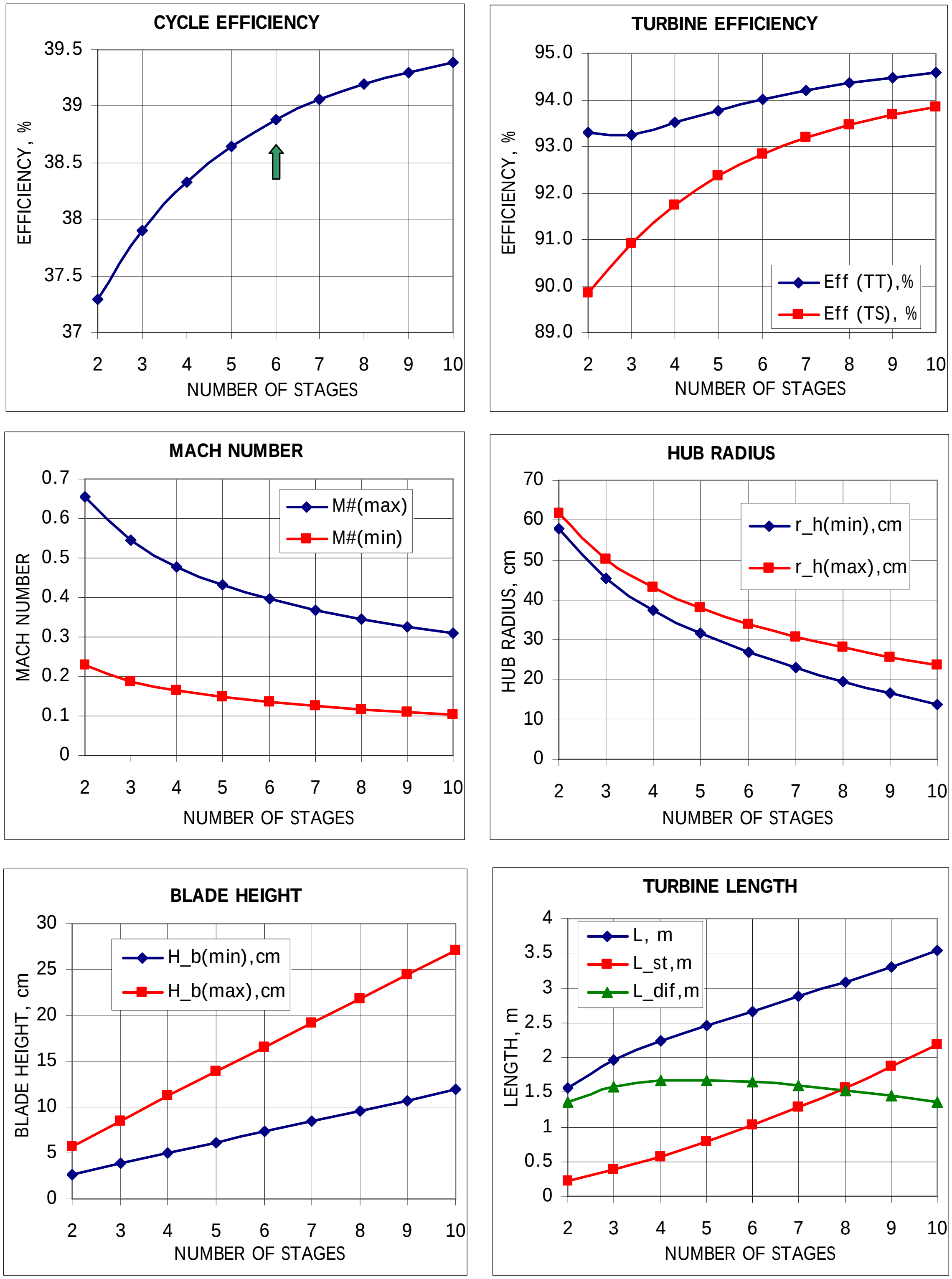

Figure 20. Turbine Optimization for the ABTR. [8]

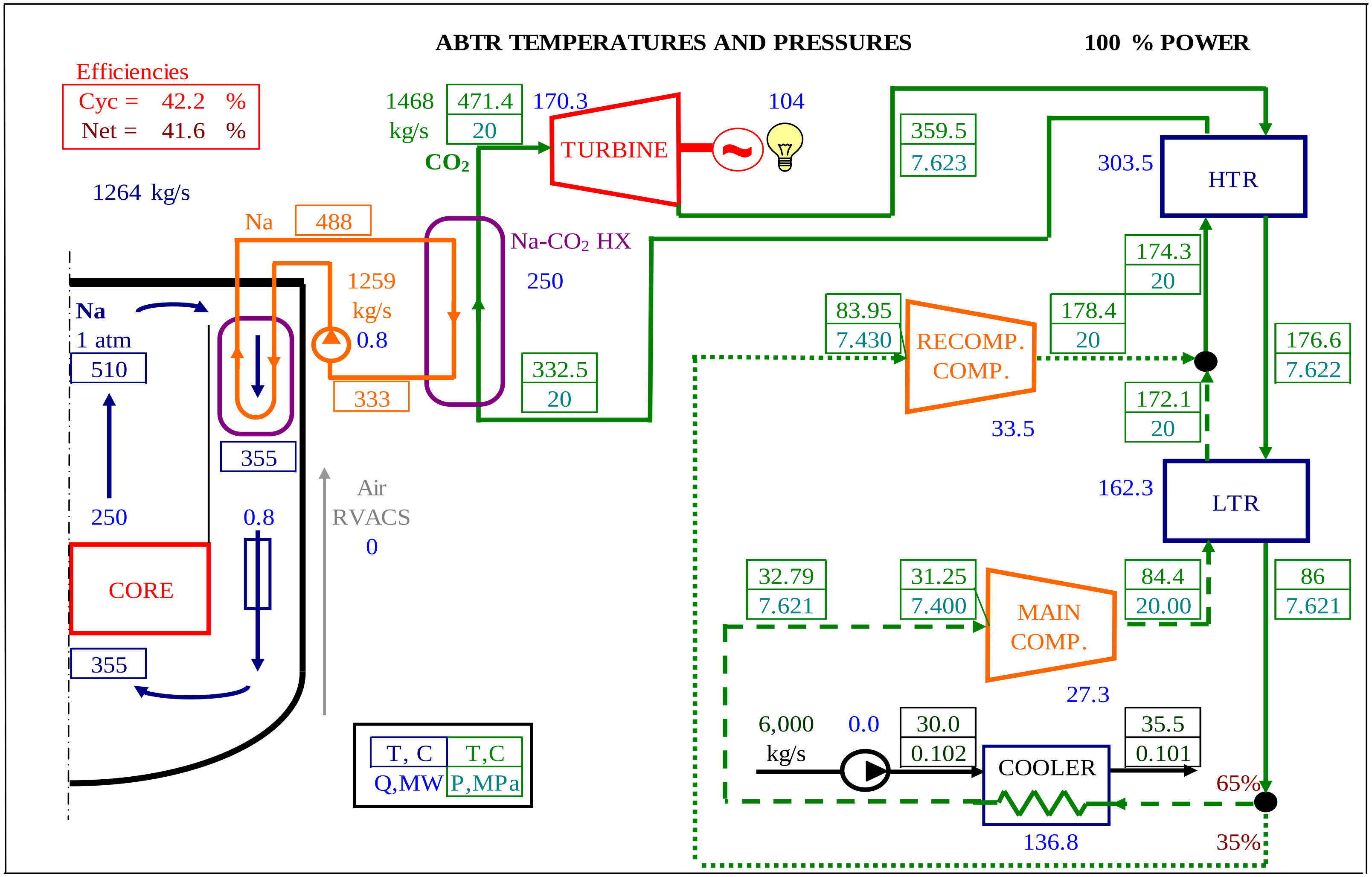

Figure 21. S-CO_2 Cycle Performance with "Ideal" Heat Exchangers.

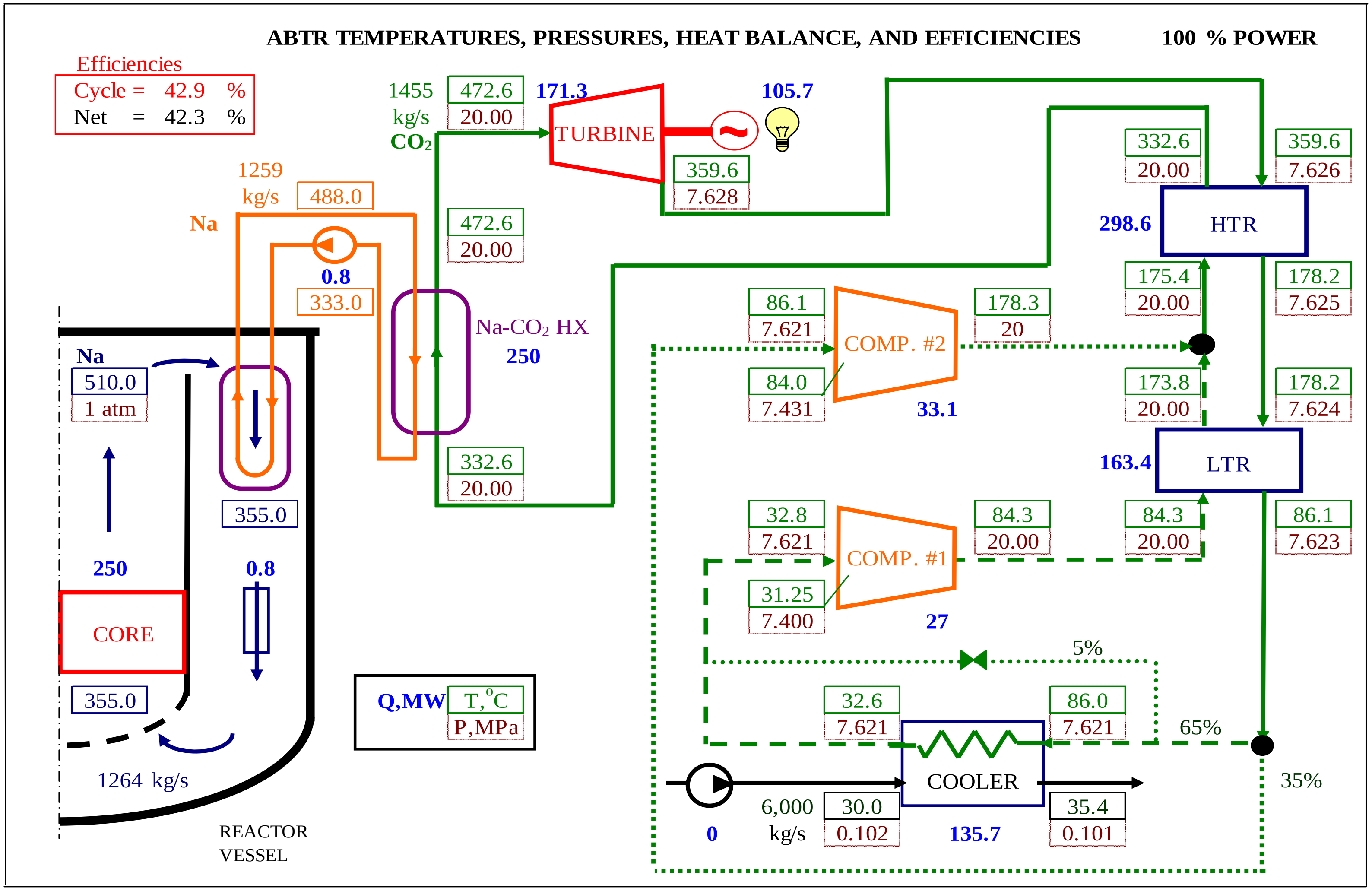

Figure 22. S-CO$_2$ Cycle Performance with "Ideal" Heat Exchangers and a 12-stage Turbine.

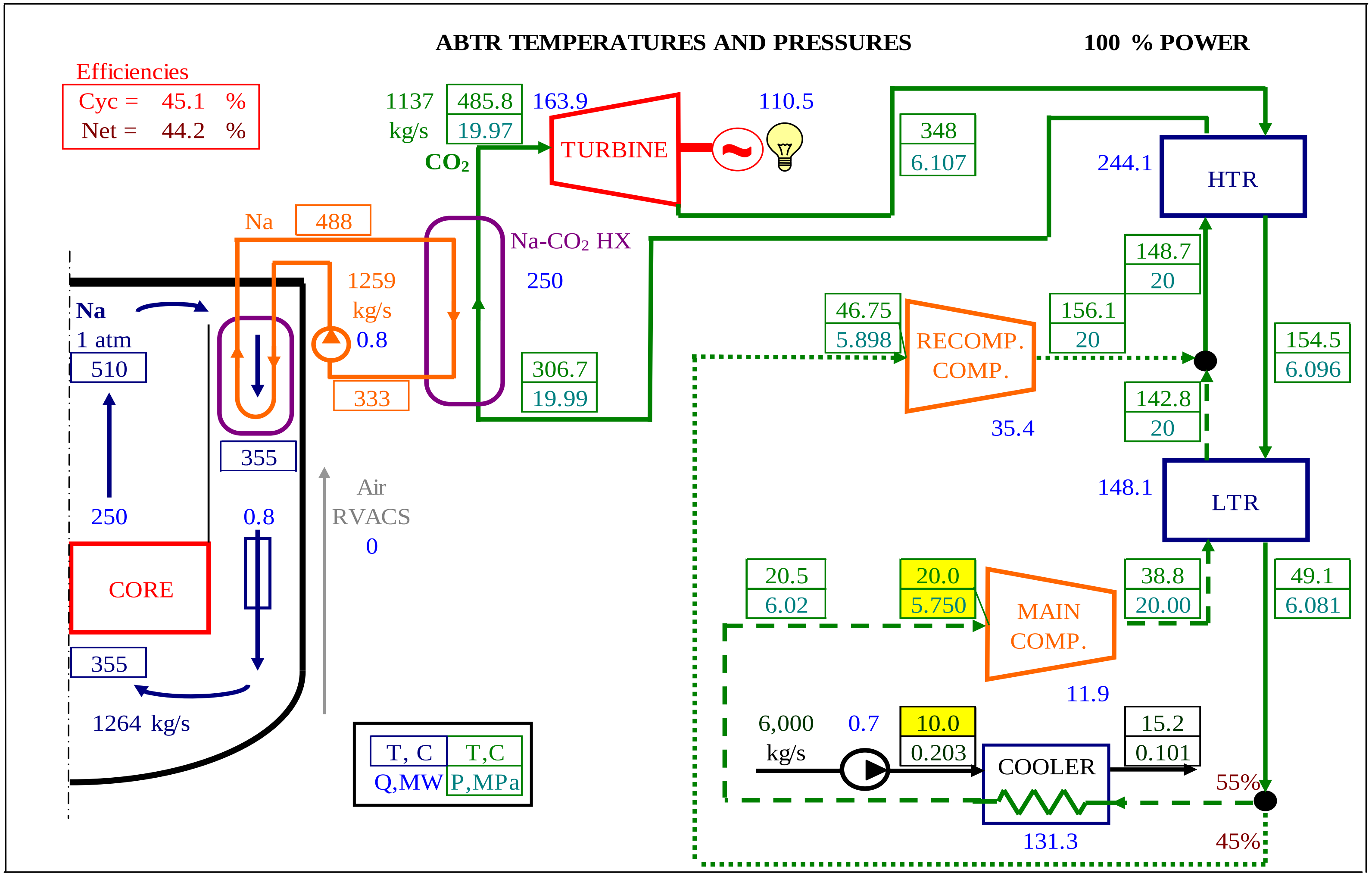

Figure 23. Performance of CO_2 Condensation Cycle with Large Components.

8. Summary

Several options for efficiency improvement for S-CO_2 Brayton cycle power conversion for a sodium-cooled fast reactor (SFR) have been investigated. The S-CO_2 Brayton cycle efficiency has been investigated for each of the options in the context of a power converter for the 250 MWt Advanced Burner Test Reactor (ABTR) concept developed at Argonne National Laboratory. The calculated efficiencies have been compared with conditions for the reference ABTR S-CO_2 Brayton cycle power converter.

Some of the options did not improve the cycle efficiency as could be anticipated beforehand. Those options include: a double recompression cycle, intercooling between the compressor stages, and reheating between the turbine stages. Among the main reasons which prevent efficiency improvement for these options are: CO_2 properties variation near the critical point, recompression cycle configuration (to partially compensate for the properties variation), and limiting sodium temperature on the low end of the sodium temperature range.

For the other group of the considered options, the current analysis confirms the possibilities of improving the cycle efficiency that have been indentified in previous investigations. The options in this group include: increasing the heat exchanger and turbomachinery sizes, raising of the cycle high end pressure (though the improvement potential of this option is very limited), and optimization of the low end temperature and/or pressure to operate as close to the (pseudo) critical point as possible.

On the other hand, the analyses carried out for this work have shown that sometimes significant cycle performance improvement can be realized if the cycle operates below the critical temperature at its low end. Such operation, however, requires the availability of a heat sink with a temperature lower than 30 ^{o}C for which applicability of this configuration is dependent upon the climate conditions where the plant is constructed (i.e., site specific). The significant improvement in cycle efficiency makes this approach worthwhile considering if site conditions allow its implementation. This approach does not favor design certification of a standard plant design that includes tropical conditions, however.

Overall, it has been shown that the S-CO_2 cycle efficiency can potentially be increased to 45 %, if a low temperature heat sink is available and incorporation of larger components (e.g.., heat exchangers or turbomachinery) having greater component efficiencies does not significantly increase the overall plant cost.

All promising options considered in this work achieve an improvement in efficiency at the expense of capital cost increase. Therefore, additional analysis is required to investigate how the options affect the overall plant economics. In other words, a tradeoff study is required to compare the costs and benefits of each option. Also, additional analysis is required to determine how options that may be attractive from the tradeoff between cost and performance enhancement viewpoint affect the controllability and safety of the entire plant.

Acknowledgments

Argonne National Laboratory's work was supported by the U. S. Department of Energy Generation IV Nuclear Energy Systems Initiative under the Work Packages, G-AN07SF0301, Energy Conversion - ANL S-CO_2 Control Analysis, and G-AN08VH0101, Energy Conversion - Brayton Cycle Control Analysis. The authors are grateful to Dr. Paul S. Pickard of Sandia National Laboratories, the Generation IV National Technical Director for Energy Conversion, Dr. Rob M. Versluis., the U.S. DOE Generation IV Program Manager, and Dr. Carl Sink, the U.S. DOE Program Manager for Energy Conversion. The authors are also indebted to Dr. Jim Cahalan, the ANL Work Package Manager for the project.

References

1. Dostal, V., Hejzlar, P., Driscoll, M. J., Todreas, N.E., 2001. A supercritical CO_2 Brayton cycle for advanced reactor applications. Trans. Am. Nucl. Soc., 85, 110-111.

2. Dostal, V., Driscoll, M. J., Hejzlar, P., Todreas, N.E., 2002. A supercritical CO_2 gas turbine power cycle for next-generation nuclear reactors, ICONE10-22192, Proceedings of ICONE-10, Arlington, Virginia, April 14-18.

3. Moisseytsev, A., Sienicki, J.J., and Wade, D.C., "Cycle Analysis of Supercritical Carbon Dioxide Gas Turbine Brayton Cycle Power Conversion System for Liquid Metal-Cooled Fast Reactors", Paper ICONE 11-36023, Proceedings of ASME International Conference on Nuclear Energy, ICONE-11, Tokyo (April 20-23, 2003).

4. Moisseytsev, A., "Passive Load Follow Analysis of the STAR-LM and STAR-H2 Systems", Ph.D. Dissertation, Texas A&M University, College Station, TX, 2003.

5. Sienicki, J. J., Moisseytsev, A. V., Wade, D. C., Farmer, M. T., Tzanos, C. P., Stillman, J. A., Holland, J. W., Petkov, P. V., Therios, I. U., Kulak, R. F., and Wu, Q., "The STAR-LM Lead-Cooled Closed Fuel Cycle Fast Reactor with a Supercritical Carbon Dioxide Brayton Cycle Advanced Power Converter", Proc. Russian Forum for Science and Technology FAST NEUTRON REACTORS Heavy Liquid Metal Coolants in Nuclear Technologies (HLMC-2003), Obninsk, Russia, Dec. 8-12, 2003.

6. Dostal, V., "A Supercritical Carbon Dioxide Cycle for Next Generation Nuclear Reactors," Dissertation, Massachusetts Institute of Technology, Department of Nuclear Engineering, January 2004.

7. Muto, Y, Private Communication with J. J. Sienicki, Tokyo Institute of Technology, February 23, 2006.

8. Chang, Y.I., et. al., "Advanced Burner Test Reactor Preconceptual Design Report," ANL-ABR-1 (ANL-AFCI-173), Argonne National Laboratory, September 5, 2006.

9. Sienicki, J. J., Moisseytsev, A., Wade, D. C., and Nikiforova, A., "Status of Development of the Small Secure Transportable Autonomous Reactor (SSTAR) for Worldwide Sustainable Nuclear Energy Supply," 2007 International Congress on Advances in Nuclear Power Plants (ICAPP 2007), Nice, May 13-18, Paper 7218.

10. Sienicki, J.J., Moisseytsev, A., Cho, D.H., Momozaki, Y., Kilsdonk, D.J., Haglund, R.C., Reed, C.B., and Farmer, M.T., "Supercritical Carbon Dioxide Brayton Cycle Energy Conversion for Sodium-Cooled Fast Reactors/Advanced Burner Reactors," Paper 181359, Global 2007: Advanced Nuclear Fuel Cycles and Systems, Boise, Idaho, September 9-13, 2007.

Appendix A.

Carbon Dioxide Temperature-Entropy and Enthalpy-Entropy Diagrams[1]

[1] The diagrams are plotted based on the data obtained from the NIST Thermophysical Properties of Fluid Systems website, http://webbook.nist.gov/chemistry/fluid/

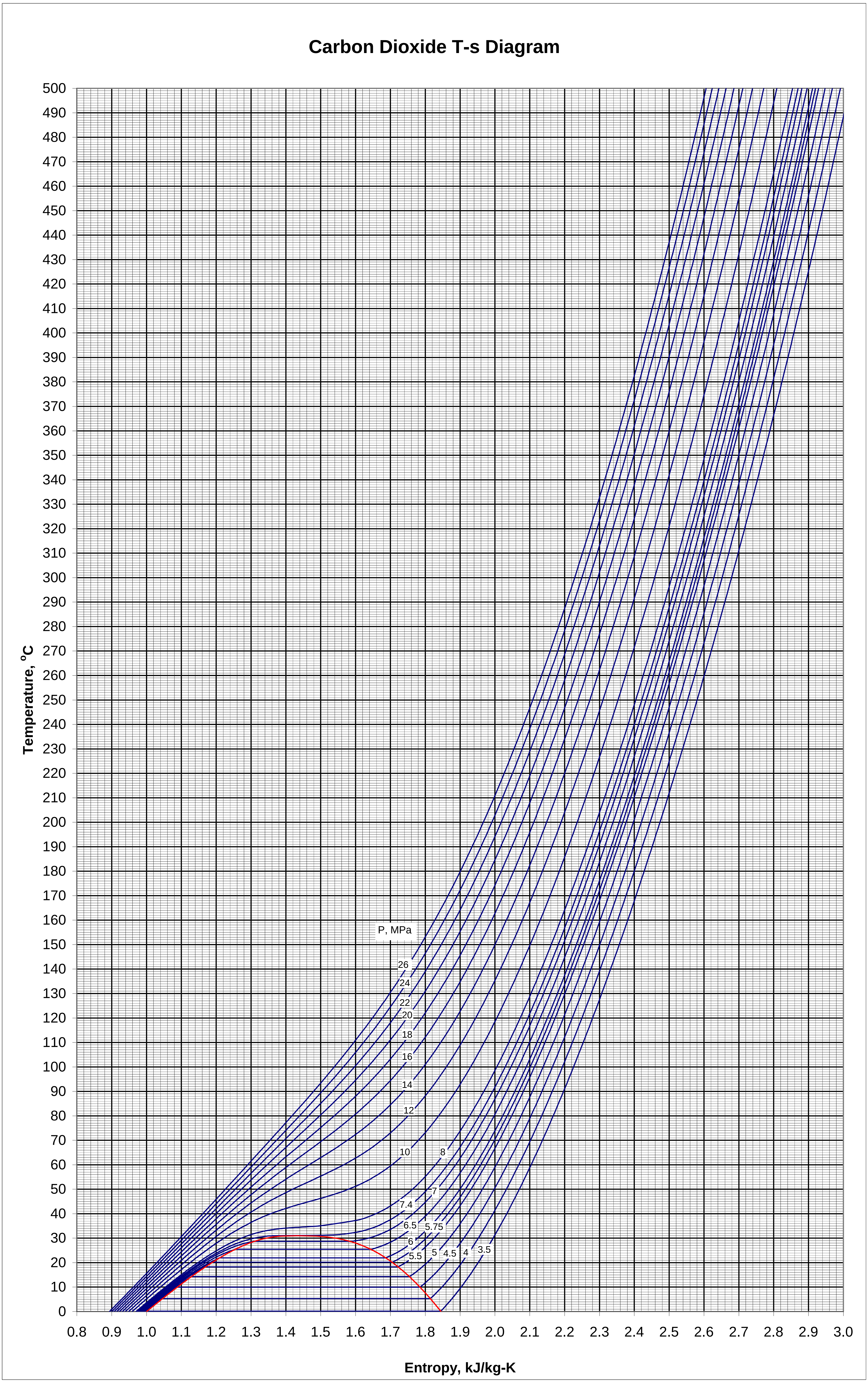
Carbon Dioxide T-s Diagram
Temperature, °C
Entropy, kJ/kg-K
P, MPa
26
24
22
20
18
16
14
12
10
8
7
7.4
6.5
5.75
6
5.5
5
4.5
4
3.5
500
490
480
470
460
450
440
430
420
410
400
390
380
370
360
350
340
330
320
310
300
290
280
270
260
250
240
230
220
210
200
190
180
170
160
150
140
130
120
110
100
90
80
70
60
50
40
30
20
10
0
0.8
0.9
1.0
1.1
1.2
1.3
1.4
1.5
1.6
1.7
1.8
1.9
2.0
2.1
2.2
2.3
2.4
2.5
2.6
2.7
2.8
2.9
3.0

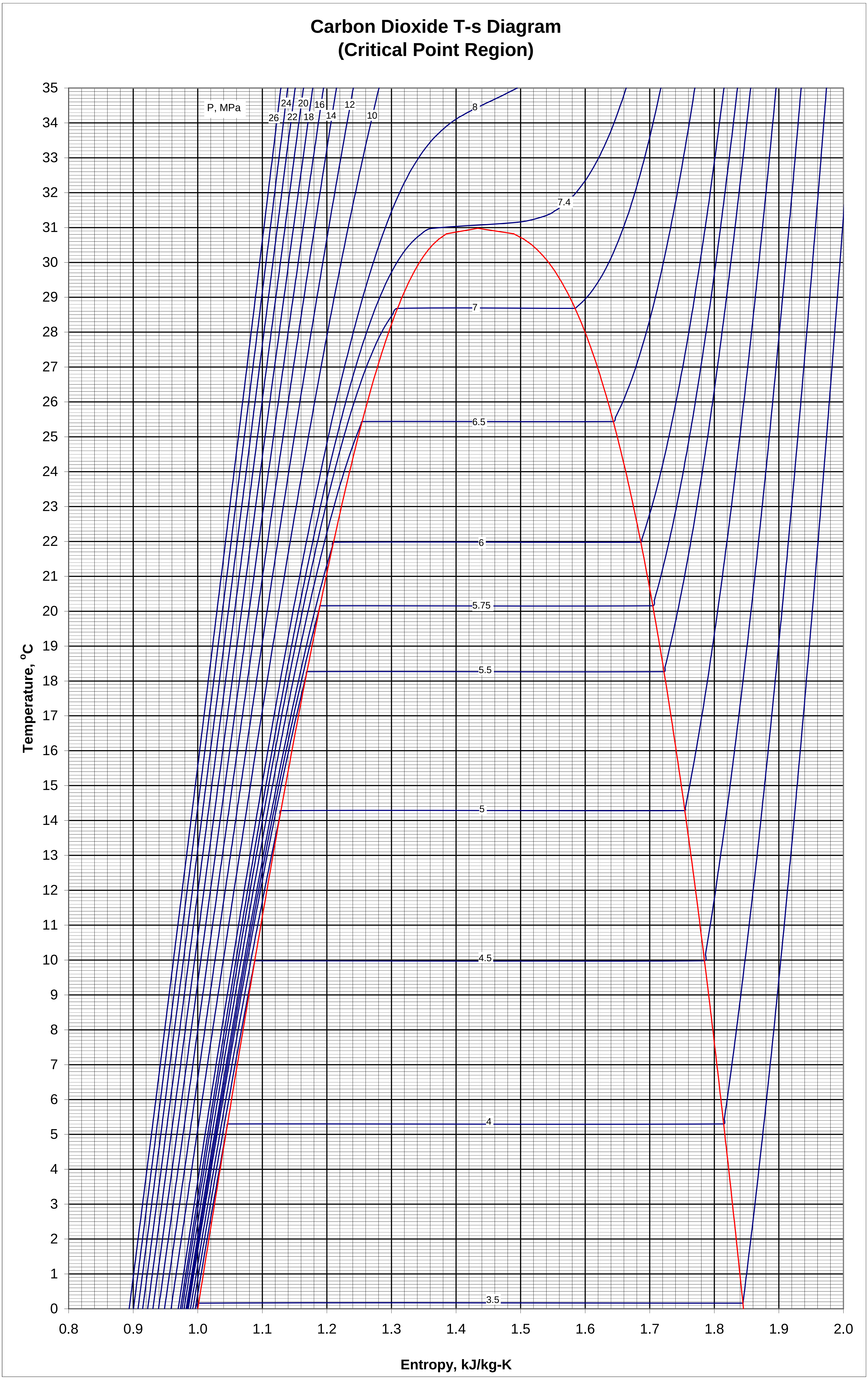

Carbon Dioxide T-s Diagram
(Critical Point Region)
P, MPa
26
24
22
20
18
16
14
12
10
8
7.4
7
6.5
6
5.75
5.5
5
4.5
4
3.5
Temperature, °C
Entropy, kJ/kg-K
0.8
0.9
1.0
1.1
1.2
1.3
1.4
1.5
1.6
1.7
1.8
1.9
2.0

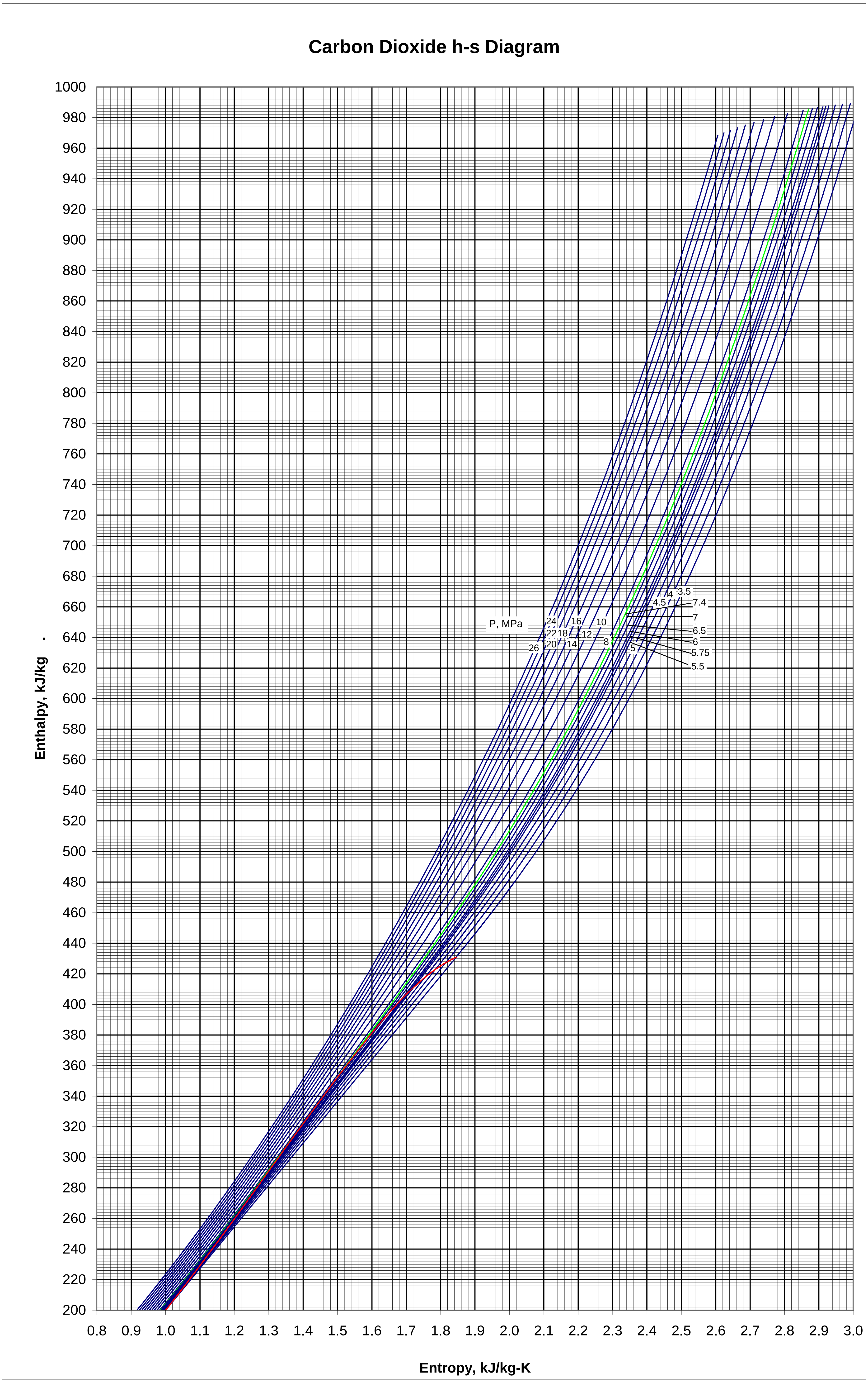
Carbon Dioxide h-s Diagram
Enthalpy, kJ/kg
Entropy, kJ/kg-K
P, MPa
26
24
22
20
18
16
14
12
10
8
7.4
7
6.5
6
5.75
5.5
5
4.5
4
3.5
1000
980
960
940
920
900
880
860
840
820
800
780
760
740
720
700
680
660
640
620
600
580
560
540
520
500
480
460
440
420
400
380
360
340
320
300
280
260
240
220
200
0.8
0.9
1.0
1.1
1.2
1.3
1.4
1.5
1.6
1.7
1.8
1.9
2.0
2.1
2.2
2.3
2.4
2.5
2.6
2.7
2.8
2.9
3.0

Nuclear Engineering Division
Argonne National Laboratory
9700 South Cass Avenue, Bldg. 208
Argonne, IL 60439-4842

www.anl.gov